

# Accelerating Spherical K-Means Clustering for Large-Scale Sparse Document Data

Kazuo Aoyama and Kazumi Saito

**Abstract**—This paper presents an accelerated spherical K-means clustering algorithm for large-scale and high-dimensional sparse document data sets. We design an algorithm working in an architecture-friendly manner (AFM), which is a procedure of suppressing performance-degradation factors such as the numbers of instructions, branch mispredictions, and cache misses in CPUs of a modern computer system. For the AFM operation, we leverage unique universal characteristics (UCs) of a data-object and a cluster’s mean set, which are skewed distributions on data relationships such as Zipf’s law and a feature-value concentration phenomenon. The UCs indicate that the most part of the number of multiplications for similarity calculations is executed regarding terms with high document frequencies (df) and the most part of a similarity between an object- and a mean-feature vector is obtained by the multiplications regarding a few high mean-feature values. Our proposed algorithm applies an inverted-index data structure to a mean set, extracts the specific region with high-df terms and high mean-feature values in the mean-inverted index by newly introduced two structural parameters, and exploits the index divided into three parts for efficient pruning. The algorithm determines the two structural parameters by minimizing the approximate number of multiplications related to that of instructions, reduces the branch mispredictions by sharing the index structure including the two parameters with all the objects, and suppressing the cache misses by keeping in the caches the frequently used data in the foregoing specific region, resulting in working in the AFM. We experimentally demonstrate that our algorithm efficiently achieves superior speed performance in large-scale documents compared with algorithms using the state-of-the-art techniques.

## I. INTRODUCTION

Large collections of text documents have been leveraged in a variety of fields. Understanding their latent structures helps us effectively utilize such document collections. Clustering is one useful method for revealing these structures. Among clustering algorithms, a  $K$ -means clustering called Lloyd’s algorithm [1], [2], which is classic yet simple and practical, has been widely used for over 50 years and has been applied to a part of various algorithms such as spectral clustering [3], [4] and neural-network compression [5], [6]. It partitions an object data set into  $K$  distinct clusters with a given number  $K$  by locally minimizing an objective function in an iterative greedy manner. For document-data sets, its specialized variant is known as a spherical  $K$ -means clustering algorithm [7], [8].

The spherical  $K$ -means clustering algorithm consists of two main steps, assignment and update, just like Lloyd’s algorithm; it differs in its given object-feature vectors and a similarity definition. Feature vector  $\mathbf{x}_i$  ( $i = 1, 2, \dots, N$ ) is

represented as a point on a unit hypersphere, i.e.,  $\|\mathbf{x}_i\|_2 = 1$ . Mean-feature vector  $\boldsymbol{\mu}_j^{[r]}$  of the  $j$ th cluster ( $j = 1, 2, \dots, K$ ), which is calculated at the update step in the  $r$ th iteration, is also normalized by its  $L_2$ -norm, resulting in  $\|\boldsymbol{\mu}_j^{[r]}\|_2 = 1$ . A similarity between an object- and a mean-feature vector is defined by the cosine similarity, which is an inner product in this case. Note that the  $j$ th cluster’s mean can be referred to as the centroid to avoid confusion with a mathematical mean.

In the spherical  $K$ -means setting, we solve a  $K$ -means clustering problem for large-scale and high-dimensional sparse document-data sets with a huge number of  $K$ . In a typical data set, we deal with the following: number of documents  $N > 1 \times 10^6$ , number of distinct terms in the data set (dimensionality)  $D > 1 \times 10^5$ , average number of distinct terms per document  $\hat{D} \sim 100$ , and  $K \sim N/100$ . For fine-grained analyses on a large-scale documents [9], a huge number of  $K$  is required in the normal course of events. Hereinafter, we respectively call data sets with  $(\hat{D}/D) \ll 1$  and  $(\hat{D}/D) \sim 1$  *sparse* and *dense*<sup>1</sup>.

Such data sets and their clustering results have interesting *universal characteristics* (UCs) of skewed forms regarding some quantities such as Zipf’s law (Section III). Among them, a *feature-value concentration phenomenon* is especially impressive, i.e., a cluster is annotated by one or a few dominant terms (words) with very large feature values. Owing to them, a relationship between a similarity and its calculation cost becomes like the Pareto principle, i.e., a large fraction of the similarity is calculated at low cost (Section III). Furthermore, a noteworthy phenomenon also appears, *initial-state independence*, i.e., an initial-state selection (seeding) for clustering does not affect algorithm’s performance, especially if a  $K$  value is large as in our setting (Section III and Appendix H). Thus, the UCs play an important role in our algorithm design and evaluation as well as can be a scientific research subject from a viewpoint of knowledge discovery.

The Lloyd’s algorithm has been improved so as to operate at high speed and the smallest possible memory size [13]–[20]. Such *accelerations* are, however, for not sparse but dense data sets in a metric space. Note that the term *acceleration* means only to speed up an algorithm while keeping the same solution as Lloyd’s algorithm if the algorithms start with identical initial states. Then clustering accuracy is no longer a performance measure. The acceleration in the foregoing algorithms originates in reducing costly exact distance calculations

<sup>1</sup>Although the definitions of *sparse* and *dense* data are vague, such language has been used in many studies in a similar manner. For instance, the indicators  $(\hat{D}/D)$  in the previous work [10], [11] are from  $2 \times 10^{-7}$  to  $4.6 \times 10^{-3}$  and that in another [12] is around  $5 \times 10^{-2}$ .

between objects and centroids with pruning methods based on the triangle inequality in a metric space.

We briefly explain a typical usage of the triangle inequality and point out its disadvantage. Consider skipping a distance calculation between object  $x_i$  and current target centroid  $\mu_j^{[r]}$  by using a lower bound on the distance. We can do it if the lower bound is larger than a distance between  $x_i$  and a centroid of the cluster which  $x_i$  is assigned to. By applying the triangle inequality to three points of  $x_i$ ,  $\mu_j^{[r]}$ , and the previous centroid  $\mu_j^{[r-1]}$ , the lower bound is calculated as

$$d_{LB}(x_i, \mu_j^{[r]}) = |d(x_i, \mu_j^{[r-1]}) - \delta_j^{[r]}|, \quad (1)$$

where  $\delta_j^{[r]}$  denotes the moving distance between  $\mu_j^{[r-1]}$  and  $\mu_j^{[r]}$  and  $d(\mathbf{a}, \mathbf{b})$  and  $d_{LB}(\mathbf{a}, \mathbf{b})$  respectively denote the distances of  $\mathbf{a}$  to  $\mathbf{b}$  and the lower bound (detailed in Appendix J). The lower bound tightens as the moving distance becomes smaller. Then more centroids are pruned, causing acceleration. However, such acceleration algorithms have an essential limit, that is, they become effective only around the last stage before the convergence where most of the centroids are invariant or slightly move. Suppose that we prepare an algorithm by replacing the distance with the cosine similarity and utilizing a similar pruning strategy for the foregoing accelerations [11]. In our setting, it is not efficient as stated above (detailed in Section II). For further improvement, it is desired that the acceleration goes through all the iterations, particularly from the early to the middle stage.

We challenge the efficient acceleration of the spherical  $K$ -means in our setting, under the condition of it operates in a modern computer system with CPUs. Our idea is to make an algorithm to operate in an *architecture-friendly manner* (AFM) through all the iterations by leveraging the universal characteristics (UCs) for *data structures* and *pruning filters*. An algorithm operating in the AFM uses as few microcode instructions issued in the CPU as possible, preventing pipeline hazards that degrade computational performance, i.e., suppressing performance-degradation factors including the multiplications for similarity calculations<sup>2</sup> (Section II).

Regarding the data structure, we employ an inverted-index data structure as in similarity search algorithms for large-scale documents [21], which utilize it for a database [22]–[26]. Our inverted index is characterized by its usage and novel structure: it is applied not to an object-feature-vector set but to a mean-feature-vector set since it effects better performance [27] and partitioned into three regions with two structural parameters (separators or thresholds) for an efficient pruning filter based on the UCs. Furthermore, an object is represented with a tuple (term ID, object-feature value) called sparse expression, where the term IDs are given in ascending order of the document frequency.

We utilize two pruning filters; a novel main and a conventional auxiliary one. The main filter exploits a unique upper bound on a similarity, which is calculated by utilizing both the *summable* property of the inner product (similarity) and

an *estimated shared* (ES) threshold on mean-feature values, based on the foregoing data structures (Sections IV and V). Besides our upper-bound-based pruning (UBP) filter, we can consider other UBP filters with the state-of-the-art techniques such as a threshold algorithm (TA) in the similarity-search field [12], [28] and blockification using the Cauchy-Schwarz inequality (CS) [29] (Section VI-D). Our UBP filter differs from the TA and CS in ways that its threshold is *estimated* by minimizing an approximate number of multiplications for similarity calculations and is *shared* with all the objects. For this reason, we call our UBP filter ES. Our auxiliary filter is called an invariant-centroid-based pruning (ICP) filter [13], [29], [30]. It becomes effective toward the last stage in the iterations. It is a sort of accelerations that uses the moving distance (Section IV-B). By combining both the filters, our algorithm works in the AFM through all the iterations.

In a similar setting to ours, an algorithm has been reported which uses a mean-inverted index and pruning filters consisting of a UBP filter based on the Cauchy-Schwarz inequality and a simpler ICP filter [9]. Our proposed algorithm is evaluated compared with similar algorithms with UBP filters based on the TA and CS combined with the auxiliary ICP filter in Section VI-D.

Note that the following strategies are out of our challenge while they are useful for speeding up: fast heuristics and approximations that don't give the same solution as Lloyd's algorithm [31], [32] and initial-state selections (seeding) that may lead to fast convergence [33]–[36] but did not affect the performance in our preliminary experiments (Section III and Appendix H). Since the strategies are orthogonal to our algorithm, they don't conflict with ours but rather can be merged into it.

Our contributions are threefold:

- 1) We propose an accelerated spherical  $K$ -means clustering algorithm for large-scale and high-dimensional document-data sets with a huge  $K$  value (Section IV). Our proposed algorithm drastically reduces the elapsed time required at the assignment step in each iteration by suppressing the performance-degradation factors including the number of multiplications. The algorithm is supported by the interrelated data structures and pruning filters based on the universal characteristics (UCs) of the data sets (Section III), resulting in its operation in the architecture-friendly manner (AFM) (Section II).
- 2) We develop an algorithm for determining two structural parameters that partition the mean-inverted index into three regions (Section V). Based on a newly introduced computational model, the algorithm simultaneously finds structural-parameter values at which the approximate number of multiplications is minimum.
- 3) We experimentally demonstrate that our proposed algorithm achieves superior performance on speed and memory consumption when it is applied to large-scale real document-data sets with large  $K$  values and compare it with other similar algorithms (Section VI).

The remainder of this paper consists of the following eight sections. Section II describes the design of both the data structure and an algorithm operating in the AFM. Section III shows

<sup>2</sup>The number of multiplications is closely related to the number of microcode instructions regarding similarity calculations and can be directly monitored in real time.

TABLE I  
NOTATION

Symbol	Description and Definitions
$N$	Number of given objects (feature vectors)
$K$	Number of clusters (means or centroids)
$D$	Dimensionality Number of distinct terms in an object data set
$\mathcal{X}$	Set of given objects (feature vectors) $\mathcal{X} = \{\mathbf{x}_1, \mathbf{x}_2, \dots, \mathbf{x}_N\}$
$\mathcal{C}^{[r]}$	Set of clusters at the $r$ th iteration $\mathcal{C}^{[r]} = \{C_1^{[r]}, \dots, C_j^{[r]}, \dots, C_K^{[r]}\}$
$a(i)$	ID of the cluster which $\mathbf{x}_i$ is assigned to
$\mathcal{M}^{[r]}$	Set of means calculated at the $r$ th iteration $\mathcal{M}^{[r]} = \{\mu_1^{[r]}, \dots, \mu_j^{[r]}, \dots, \mu_K^{[r]}\}$ $\mu_{a(i)}^{[r]}$ : Mean of $C_{a(i)}^{[r]}$ which $\mathbf{x}_i$ is assigned to
$\rho$	Set of similarities between an object and centroids $\rho = \{\rho_1, \rho_2, \dots, \rho_K\}$ , $\rho_{(max)} = \max_{1 \leq j \leq K} (\rho_j)$ $\rho_{a(i)}$ : Similarity of $\mathbf{x}_i$ to $\mu_{a(i)}$ . Object ID is omitted from each symbol $\rho_j$ .
$\hat{D}$	Average number of distinct terms in sparse object data set $\mathcal{X}$ , $\hat{D} = (1/N) \sum_{i=1}^N (nt)_i$
$\mathcal{S}$	Set of term IDs, $s \in \mathcal{S}$ , $ \mathcal{S}  = D$
$\hat{\mathcal{X}}$	Set of object-tuple arrays of $\hat{\mathbf{x}}_i$ , $i = 1, 2, \dots, N$ $\hat{\mathbf{x}}_i = [(t_{(i,p)}, u_{t_{(i,p)}})]_{p=1}^{(nt)_i}$ $t_{(i,p)}$ : $p$ th term ID appeared in $\hat{\mathbf{x}}_i$ Term ID's are sorted in ascending order of document frequency ( $df$ ) $u_{t_{(i,p)}}$ : $p$ th feature value appeared in $\hat{\mathbf{x}}_i$ $(nt)_i$ : Number of distinct terms in $\hat{\mathbf{x}}_i$
$\check{\mathcal{M}}^{[r]}$	Structured inverted index of means, each column of which is mean-tuple array $\check{\xi}_s^{[r]}$ , $s = 1, 2, \dots, D$ $\check{\xi}_s^{[r]} = [(c_{(s,q)}, v_{c_{(s,q)}})]_{q=1}^{(mf)_s}$ $c_{(s,q)}$ : $q$ th mean ID appeared in $\check{\xi}_s^{[r]}$ $v_{c_{(s,q)}}$ : $q$ th feature value appeared in $\check{\xi}_s^{[r]}$ $(mf)_s$ : Mean frequency of $s$ th term ID

the UCs of a large-scale high-dimensional sparse document-data set and its clustering results. Section IV explains our proposed algorithm in detail, and Section V describes how to estimate the two structural parameters that are separators of the mean-inverted index. Section VI shows our experimental settings and compares our algorithm's performance with others. Section VII discusses our proposed clustering algorithm based on experimental results, and Section VIII reviews related work from viewpoints that clarify the distinct aspects of our work. The final section provides a conclusion and future work.

For convenience, we list the notation in Table I.

## II. ARCHITECTURE-FRIENDLY MANNER

We consider running an algorithm on a modern computer system with CPUs. An architecture-friendly manner (AFM) is a procedure that suppresses the following three performance-degradation factors: (1) the instructions, (2) the conditional branch mispredictions, and (3) the cache misses. These factors impact the performance of algorithms executed on a modern computer system, which contains CPUs and a hierarchical memory system as its main components. A CPU has plural operating cores each of which has deep pipelines for instruction parallelism with superscalar out-of-order execution and multilevel cache hierarchy [37], [38]. The memory system

## Algorithm 1 Assignment step of MIVI

---

**Input:**  $\hat{\mathcal{X}}$ ,  $\check{\mathcal{M}}^{[r-1]}$ ,  $\{\rho_{a(i)}^{[r-1]}\}_{i=1}^N$ ,  $\forall j$ ;  $C_j^{[r]} \leftarrow \emptyset$

**Output:**  $\mathcal{C}^{[r]} = \{C_j^{[r]}\}_{j=1}^K$

- 1: **for all**  $\hat{\mathbf{x}}_i = [(t_{(i,p)}, u_{t_{(i,p)}})]_{p=1}^{(nt)_i}$ ,  $|\hat{\mathcal{X}}| = N$  **do**
- 2:    $\{\rho_j\}_{j=1}^K \leftarrow 0$ ,  $\rho_{(max)} \leftarrow \rho_{a(i)}^{[r-1]}$
- 3:   **for all**  $[t_{(i,p)}]_{p=1}^{(nt)_i}$  **do**
- 4:     **for all**  $[v_{c_{(s,q)}}]_{q=1}^{(mf)_s} \in \check{\xi}_s^{[r-1]}$ ,  $s = t_{(i,p)}$  **do**
- 5:        $\rho_{c_{(s,q)}} \leftarrow \rho_{c_{(s,q)}} + u_s \cdot v_{c_{(s,q)}}$
- 6:   **for**  $j \leftarrow 1$  **to**  $K$  **do**
- 7:     **if**  $\rho_j > \rho_{(max)}$  **then**  $\rho_{(max)} \leftarrow \rho_j$ ,  $a(i) \leftarrow j$
- 8:    $C_{a(i)}^{[r]} \leftarrow C_{a(i)}^{[r]} \cup \{\hat{\mathbf{x}}_i\}$

---

TABLE II  
PERFORMANCE RATES OF DIVI AND DING<sup>+</sup> TO MIVI.

Algo	Avg Mult	Avg time	Inst	BM	LLCM
DIVI	1.000	10.21	0.9824	6.981	36.48
Ding <sup>+</sup>	0.2284	2.892	0.6533	492.9	37.23

consists of registers, hierarchical caches from level 1 to the last level (e.g., level 3) [38], and an external main memory. To efficiently run an algorithm at high throughput on the system, we should not only reduce instructions but also avoid pipeline hazards that cause pipeline stalls. In pipeline hazards, there are two serious threats: a control hazard induced by branch mispredictions [39], [40] and a data hazard that needs access to the main memory by last-level-cache misses [37]. Suppressing the three performance-degradation factors creates a high-performance algorithm.

We describe the impact of branch mispredictions and last-level-cache misses, comparing the following three algorithms. A baseline algorithm utilizes an inverted-index data structure for a mean (centroid) set and adopts the term-at-a-time (TAAT) strategy [41] for similarity calculations, which is called a mean-inverted-index algorithm (MIVI) in Algorithm 1 [27]. The second differs from MIVI only in using an inverted index for a given data-object set, which is called a data-inverted-index algorithm (DIVI). The last is an algorithm Ding<sup>+</sup> [18], which is originally for dense data sets and works at high speed using its pruning filters based on the triangle inequality. To make Ding<sup>+</sup> available to a sparse data set in the spherical  $K$ -means setting, we modified it without any inverted index as follows. A given data-object and a mean set were represented with sparse and full expression, respectively. In the full expression, all the term IDs were covered, where feature values of undefined term IDs were filled by zeros. These representations enable us to simply and quickly access a mean-feature value by using a data-object term ID as a key for a similarity calculation<sup>3</sup>. As is obvious, Ding<sup>+</sup> used a cosine similarity as with an algorithm [11] that is modified from Hamerly's algorithm [15].

Figure 1 and Table II show the performance comparisons of MIVI, DIVI, and Ding<sup>+</sup> in the 8.2M-sized PubMed data set

<sup>3</sup>Mean-feature vectors may also be represented with sparse expression. However, these representations require solving a set-intersection problem of finding terms shared by both a data-object- and a mean-feature vector.

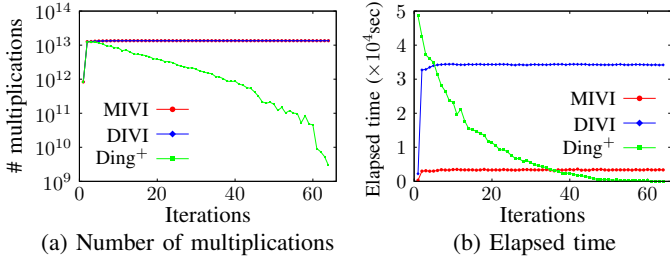


Fig. 1: Performance comparison of MIVI, DIVI, and Ding<sup>+</sup> in 8.2M-sized PubMed data set with  $K=80\,000$ : (a) Number of multiplications and (b) Elapsed time along iterations.

(Section VI-A) [42] with  $K = 80\,000$  until the convergence. The performance rates of DIVI and Ding<sup>+</sup> to MIVI are shown in Table II. The columns from left to right show the algorithm (Algo), the average number of multiplications (Avg Mult), the average elapsed time (Avg time), the numbers of completed instructions (Inst), branch mispredictions (BM), and last-level-cache load misses (LLCM). The entries in the last three columns were measured with Linux perf tools [43].

Both MIVI and DIVI required an identical number of multiplications for similarity calculations. However, their average elapsed times were critically different. Surprisingly, DIVI needed almost 10 times more average elapsed time than MIVI. Ding<sup>+</sup> reduced the multiplications by its pruning method, resulting in almost one-fourth the average number of MIVI’s multiplications. However, its average elapsed time was about three times larger than MIVI’s. These results reveal that only the number of multiplications or instructions is insufficient for the speed-performance criterion.

Table II also shows that the numbers of branch mispredictions and cache misses of DIVI and Ding<sup>+</sup> were significantly larger than those of MIVI. The branch misprediction and the cache miss cause many wasted clock-cycle times, resulting in slower operation. This can be explained as follows. When a target-data-object does not exist in the caches, a last-level-cache miss occurs and the object is loaded from the main memory in the large memory latency. Such a situation is generally caused by the poor temporal and spatial locality in data usage. DIVI replaces the triple loop of MIVI at lines 1 to 5 in Algorithm 1 as follows: the outermost loop is for mean-feature vectors, the middle loop is for the terms in a mean-feature vector whose number is much larger than  $(nt)_i$  of MIVI, and the innermost loop is for object-inverted-index arrays whose length is much longer than  $(mf)_s$  of  $\xi_s^{[r-1]}$  in MIVI (symbols in Table I). This replacement loses the locality of target data. Ding<sup>+</sup>, in a broad sense, replaces the middle and innermost loop with loops for mean-feature vectors and term IDs in  $\hat{x}_i$ , respectively, although it is technically different from MIVI in the loop structure [18]. Then, Ding<sup>+</sup> accesses a large array of the mean-feature vector in the innermost loop. The large arrays in the middle and innermost loops diminish the foregoing locality. Furthermore, Ding<sup>+</sup> uses many irregular conditional branches in several pruning filters for reducing the multiplications. When a conditional branch irregularly changes its judgment result, True or False, the branch prediction fails. Then, a series of instructions executed under the prediction is

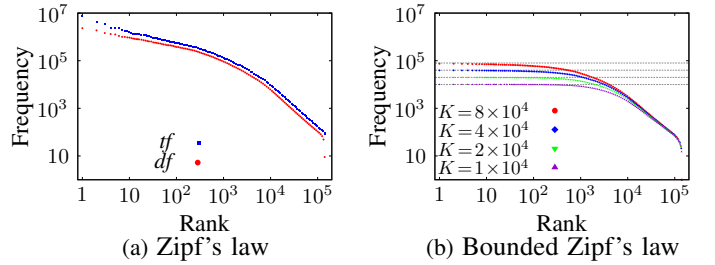


Fig. 2: Characteristics of 8.2M-sized PubMed data set: (a) Zipf’s law on term frequency ( $tf$ ) and document frequency ( $df$ ) and (b) Bounded Zipf’s law on mean frequency ( $mf$ ) with four  $K$  values.

flushed out and correct instructions are executed again. This procedure requires more clock-cycle times.

From these facts, we know that it is important for an algorithm’s AFM operation to avoid using large arrays and irregular conditional branches in deeper loops. Our proposed algorithm employs a mean-inverted index like MIVI and gives to the index a specific structure that is shared with all the objects to avoid irregular conditional branches. The structure is designed so as to keep the locality of frequently used data. Furthermore, our algorithm exploits a novel pruning filter for skipping unnecessary multiplications for similarity calculations (Section IV). These lead to suppress the performance-degradation factors.

### III. UNIVERSAL CHARACTERISTICS

Large-scale document data sets, which are generally high-dimensional and sparse, and their clustering results have universal characteristics of skewed forms regarding *some quantities*. This section describes the characteristics of such a data set and a mean (centroid) set built by  $K$ -means clustering, making connections with both the number of multiplications and the fractions of a similarity. These play an important role in designing our proposed algorithm.

The Zipf’s law is known as one of universal characteristics [44]–[46]. It states that a relationship between an occurrence frequency of a term (or word) in a text corpus (document data set) and the term’s rank in descending order of the frequency is empirically represented in a rank range by

$$Freq(\text{term}) \propto Rank(\text{term})^{-\alpha}, \quad (2)$$

where the functions,  $Freq(\text{term})$  and  $Rank(\text{term})$ , are the frequency and rank of the term, and  $\alpha$  is a positive exponent. In very large data sets, unlike the foregoing simple Zipf’s law, it is known that a rank-frequency plot in log-log scale has two parts with different exponents [47].

Figure 2(a) shows Zipf’s law of the 8.2M-sized PubMed data set (Section VI-A), where  $tf$  and  $df$  respectively denote the total occurrence frequency of each term in all of the documents and the number of documents in which each term appeared. We know that what follows Zipf’s law was not only the term frequency ( $tf$ ), which is usually said, but also the document frequency ( $df$ ). Figure 2(b) shows the relationship between the mean frequency ( $mf$ ) and  $Rank(\text{term})$ , where  $mf$  is the number of means (centroids) in which a distinct term appeared.

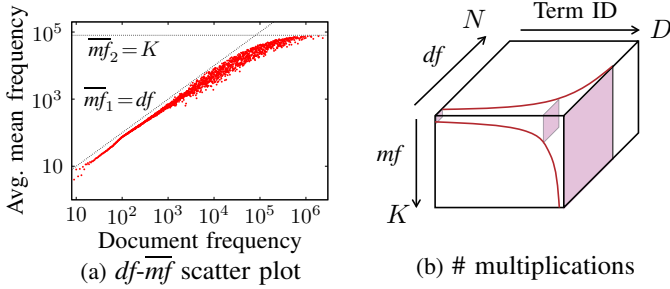


Fig. 3: Characteristics of 8.2M-sized PubMed data set: (a)  $df$ - $\overline{mf}$  scatter plot in log-log scale and (b) Diagram of number of multiplications when MIVI is executed, which corresponds to volume surrounded by curves inside the rectangle.

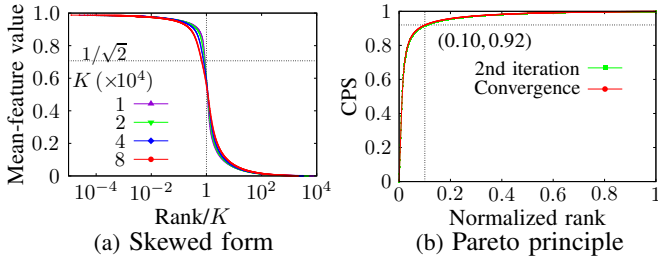


Fig. 4: (a) Skewed form of mean-feature values and (b) cumulative partial similarity (CPS) against normalized rank. Both were built from 8.2M-sized PubMed data set and  $K=80000$  was used for (b).

The log-log plots indicates that although the maximum mean frequencies were bounded by the corresponding  $K$  values, the relationship in the mean set also followed Zipf’s law, which we call a bounded Zipf’s law. The relationships in Figs. 2(a) and (b) are highly right-skewed forms expressed by power functions with negative exponents.

Figure 3(a) shows a positive correlation between  $df$  and  $\overline{mf}$  in the scatter plot in log-log scale when  $K=8 \times 10^4$  in Fig. 2, where  $\overline{mf}$  is the average mean frequency of terms having an identical document frequency, which is expressed by

$$\overline{mf} = (1/|\mathcal{S}_{df}|) \sum_{s \in \mathcal{S}_{df}} mf_s, \quad \mathcal{S}_{df} = \{s \mid df_s = df\}. \quad (3)$$

The slope of the diagonal straight line denotes  $\overline{mf}_1 = df$  and the horizontal line  $\overline{mf}_2 = K$ . This indicates that a high- $df$  term has a high  $mf$ . Figure 3(b) shows a diagram representing the number of multiplications for similarity calculations ( $\sum_{s=1}^D mf_s \cdot df_s$ ) when MIVI in Section II is applied to the data in our setting. The horizontal axis depicts the term ID given in ascending order of  $df$ , which is the opposite direction of the terms in Fig. 2(a), the depth axis represents  $df$ , and the vertical axis  $mf$ . The volume surrounded by curves inside the rectangle corresponds to the number of multiplications. This number is *quite unevenly distributed* in the large term-ID range, i.e., in the high- $df$  region.

Next, we describe skewed forms relating with the fractions of a similarity. We observed that most of clusters’ means had one or a few dominant terms with very large feature values, which is named a *feature-value concentration phenomenon* (related to Fig. 9). Figure 4(a) shows a skewed form on the feature values in all the centroids (bag-of-features), where each

feature is expressed by  $tf$ - $idf$  in Section VI-A. All the non-zero elements were sorted in descending order of their values, and the values were depicted along the rank normalized by  $K$ . Qualitatively, there exist very large feature values, and many feature vectors have them. Since no feature vector has plural elements whose values are larger than  $(1/\sqrt{2})$ , the rank at this value corresponds to the number of centroids with the larger feature values. This shows the feature-value concentration phenomenon that a very small number of features occupied a large part of feature values in each centroid. Here, consider constructing a mean-inverted index whose array is sorted by its feature values in descending order. Then, another skewed form appears in the inverted-index array, where the top to a few entries have very large feature values (Fig. 9).

The foregoing characteristics create a Pareto-principle-like phenomenon on a relationship between a cumulative partial similarity ( $CPS$ ) and a normalized rank ( $NR$ ) of the partial similarity, where the partial similarity is the product of an object- and a mean-feature value on a term and the  $NR$  is the partial-similarity rank in descending order that is normalized by the corresponding similarity (detailed in Appendix I). Figure 4(b) shows the relationship in the 8.2M-sized PubMed with  $K=80000$ . Only the 10% partial-similarity calculations led to the 92%  $CPS$ . This phenomenon indicates that a large fraction of similarity is obtained by a few multiplications. Based on this, we can make a tight upper bound on the similarity efficiently.

We call the skewed forms, which are represented as (1) Zipf’s law, (2) bounded Zipf’s law, (3) feature-value concentration phenomenon, and (4) Pareto-principle-like phenomenon, the universal characteristics of large-scale sparse data sets. We identify the special region in a mean-inverted index by utilizing newly introduced two structural parameters in Section V and structure the index. By using the structured mean-inverted index, we can exploit the UCs to reduce the multiplications for similarity calculations in Section IV.

#### IV. PROPOSED ALGORITHM: ES-ICP

Our proposed algorithm ES-ICP prunes centroids that cannot be the most similar one to reduce the multiplications for similarity calculations (more exactly, the multiply-add operations). ES-ICP utilizes both a main and an auxiliary filter. The former is a unique upper-bound-based pruning (UBP) filter named ES. Our ES filter utilizes a tight upper bound obtained with low computational cost and safely narrows down the target centroids for similarity calculations through all the iterations until convergence. The auxiliary filter is an invariant-centroid-based pruning (ICP) filter [13], [29], [30], [48] that effectively works toward the end of the iterations, which is a good match with generic algorithms using an inverted index. This section explains our algorithm with both the filters from the viewpoint of how it exploits the universal characteristics (UCs) in Section III and works in the architecture-friendly manner (AFM) in Section II.

##### A. ES Filter Design

Our ES filter does not use either the triangle inequality in a metric space or its variants; it uses the summable property

TABLE III  
NOTATION IN ES-ICP ALGORITHM

Symbol	Description and Definitions
$t^{[th]}$	Parameter: Threshold on term ID
$v^{[th]}$	Parameter: Threshold on mean-feature-value
$(mfH)_s$	Mean frequency of $s$ th term ID where $v_{(s,q)} \geq v_h^{[th]}$ : $(mfL)_s = (mf)_s - (mfH)_s$
$y_{(i,j)}$	Partial $L_1$ -norm of object-feature-vectors whose tuple $(t_{(i,p)}, u_{t_{(i,p)}})$ satisfies $t_{(i,p)} \geq t^{[th]}$ and that vary depending on the $j$ th centroid's feature value $1 \leq p \leq (nt)_{i,j}$ , $1 \leq i \leq N$ , and $1 \leq j \leq K$
$Z_i$	Set of candidate-mean ID's which is used at verification phase
$\check{\mathcal{M}}^{p[r]}$	Inverted index of partial mean-feature-vectors, each column of which is a value array with full expression, $1 \leq j \leq K$ , denoted by $\check{\zeta}_s^{[r]}$ , $t^{[th]} \leq s \leq D$
$w_{(j,s)}$	Value $w_{(j,s)} \in \check{\zeta}_s^{[r]}$ is $v_{c_{(s,q)}}$ for $c_{(s,q)} = j$ if defined and $v_j < v^{[th]}$ , 0 otherwise.
$xState$	Boolean flag for each object: 1 if it satisfies the condition in Eq. (5), otherwise 0.
$(nMv)$	Number of moving centroids
$(mfM)_s$	Mean frequency of moving centroids (means) In Region 2, only centroids satisfying $v_{c_{(s,q)}} \geq v^{[th]}$ are counted.

(or additivity) in the inner product of the cosine similarity. To construct the ES filter, we first provide structures to a given data-object and a mean set. In the data-object set, the term IDs ( $1 \leq s \leq D$ ) are sorted in ascending order of the term's document frequency ( $df$ ). An inverted-index data structure is applied to the mean set (Section II) and each array  $\check{\xi}_s$  in the mean-inverted index  $\check{\mathcal{M}}$  is aligned along term-ID  $s$  (Fig. 3(b)). Then, from the correlation between  $df$  and  $mf$  in Fig. 3(a), frequently used mean-feature values collect in the arrays with the large term IDs. To identify the arrays, we introduce a structural parameter of  $t^{[th]}$  on term IDs. Furthermore, to exploiting the feature-value concentration phenomenon, we incorporate another structural parameter of  $v^{[th]}$  on mean-feature values. The two structural parameters partition  $\check{\mathcal{M}}$  into the following three regions:

[Region 1]  $1 \leq s < t^{[th]}$  with respect to term ID ( $s$ )

[Region 2]  $t^{[th]} \leq s \leq D$  and  $v_{c_{(s,q)}} \geq v^{[th]}$ , where  $v_{c_{(s,q)}}$  is the mean-feature value of the cluster ID of  $c_{(s,q)}$ <sup>4</sup> and  $q$  is the local order ( $q = 1, \dots, (mfH)_s$ ) on  $\check{\xi}_s$  (symbols in Tables I and III)

[Region 3]  $t^{[th]} \leq s \leq D$  and  $v_{c_{(s,q)}} < v^{[th]}$ .

By setting  $t^{[th]}$  and  $v^{[th]}$  at appropriate values in Section V, we make a tight upper bound on a similarity of  $\hat{x}_i$  to mean-feature vectors, which realizes the Pareto-principle-like phenomenon in Sections III and VII. Figure 5 shows a diagram of the mean-inverted index  $\check{\mathcal{M}}$  partitioned into the three regions and its array  $\check{\xi}_s$  in Regions 2 and 3<sup>5</sup>.

Next, we define a tight upper bound based on the data structure and the additivity of the inner product. Given the  $i$ th object, we calculate the exact partial similarities to the  $j$ th

<sup>4</sup> $v_{c_{(s,q)}}$  is not sorted but only classified by a comparison to  $v^{[th]}$ .

<sup>5</sup>The entries in Region 3 are not used. Instead, a partial mean-inverted index  $\check{\mathcal{M}}^{p[r]}$  in Table III is used for calculating an exact partial similarity.

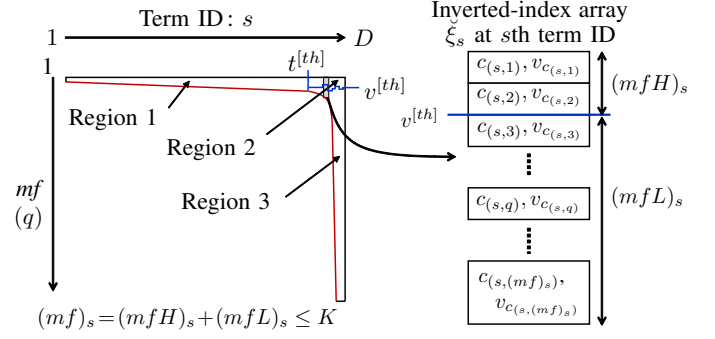


Fig. 5: Diagram of three regions illustrated on plane of term ID and mean-inverted index. Right figure represents  $s$ th mean-inverted-index array composed of tuples  $(c_{(s,q)}, v_{c_{(s,q)}})$ .

centroid;  $(\rho 1)_{(j;i)}$  and  $(\rho 2)_{(j;i)}$  in Regions 1 and 2, respectively. The upper-bound  $(\rho 3)_{(j;i)}^{[ub]}$  in Region 3 is estimated as  $\{y_{(i,j)} \cdot v^{[th]}\}$ <sup>6</sup>, where  $y_{(i,j)}$  denotes the remaining  $L_1$ -norm of  $\hat{x}_i$  which is not used in Regions 1 and 2. The upper bound on similarity  $\rho_{(j;i)}^{[ub]}$  is defined by

$$\rho_{(j;i)}^{[ub]} = (\rho 1)_{(j;i)} + (\rho 2)_{(j;i)} + (\rho 3)_{(j;i)}^{[ub]}. \quad (4)$$

Collecting frequently used mean-feature values in Region 2 leads to reducing cache misses. Limiting the inexact part to the partial similarity in Region 3 makes the upper bound tight and reduces the multiplications, i.e., the instructions. Furthermore, sharing  $t^{[th]}$  and  $v^{[th]}$  in all the objects omits unnecessary conditional branches, resulting in reducing branch mispredictions. At the verification phase, only for the  $j$ th centroid passing through the ES filter with low probability, the exact partial similarity  $(\rho 3)_{(j;i)}$  in Region 3 is calculated, using additional partial mean-inverted index  $\check{\mathcal{M}}^{p[r]}$  in Table III, whose memory size of  $\{K(D - t^{[th]} + 1)(\text{sizeof}(\text{double}))\}$ -byte is not so large because  $t^{[th]}$  is close to  $D$ . Then,  $(\rho 3)_{(j;i)}$  is added to  $(\rho 1)_{(j;i)} + (\rho 2)_{(j;i)}$  for exact similarity.

Thus, we design the ES filter with a tight upper bound on the similarity, exploiting both the UCs and the summable property of the inner product and leveraging the data structures for the algorithm's operation in the AFM.

## B. ES-ICP Algorithm

Our ES-ICP algorithm simultaneously utilizes the ES and ICP filters. The ICP filter omits the similarity calculations between the *more similar object* and the invariant centroids. The  $i$ th object is *more similar* if its similarity to the centroid whose ID is  $a(i)$  satisfies

$$\rho_{(a(i);i)}^{[r-1]} \geq \rho_{(a(i);i)}^{[r-2]}. \quad (5)$$

To make the ICP filter operate in the AFM, we furthermore provide another structure for the mean-inverted index  $\check{\mathcal{M}}^{[r]}$

<sup>6</sup>In our implementation,  $\{y_{(i,j)} \cdot v^{[th]}\}$  is not performed for reducing the multiplications (Appendix A). Instead, by  $v^{[th]}$ , object-feature values are multiplied and mean-feature values are divided, just after  $t^{[th]}$  and  $v^{[th]}$  are determined. Then, we can simply use the scaled  $\{y_{(i,j)}\}$  keeping their other products identical. This scaling becomes possible since  $v^{[th]}$  is shared with all the objects.

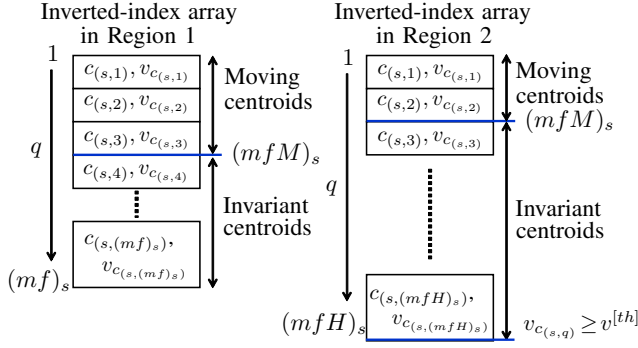


Fig. 6: Structures of mean-inverted-index arrays: Left and right figures represent  $s$ th arrays in Regions 1 and 2.

---

### Algorithm 2 Assignment step in ES-ICP algorithm

---

**Input:**  $\hat{\mathcal{X}}, \check{\mathcal{M}}^{[r-1]}, \check{\mathcal{M}}^{p[r-1]}, \{\rho_{a(i)}^{[r-1]}\}_{i=1}^N, t^{[th]}, v^{[th]}$

**Output:**  $\mathcal{C}^{[r]} = \{C_j^{[r]}\}_{j=1}^K$

▷ Calculate similarities in parallel wrt  $\hat{\mathcal{X}}$

- 1:  $C_j^{[r]} \leftarrow \emptyset, j = 1, 2, \dots, K$
  - 2: **for all**  $\hat{\mathbf{x}}_i = [(t_{(i,p)}, u_{t_{(i,p)}})]_{p=1}^{(nt)_i} \in \hat{\mathcal{X}}$  **do**
  - 3:  $\{\rho_j\}_{j=1}^K \leftarrow 0, \rho_{(max)} \leftarrow \rho_{a(i)}^{[r-1]}, \mathcal{Z}_i \leftarrow \emptyset$
  - 4: **for**  $j \leftarrow 1$  **to**  $K$  **do**
  - 5:  $y_{(i,j)} \leftarrow \sum_{t_{(i,p)} \geq t^{[th]}} (u_{t_{(i,p)}})$  ▷ Initializing  $y_{(i,j)}$
  - ▷ Gathering phase
  - 6: **if**  $x.State = 1$  **then** ▷ ICP filtering
  - 7:  $(\mathcal{Z}_i, \{\rho_j\}_{j=1}^K) = G_1(\text{args}_1)$  ▷ Algorithm 3
  - 8:  $\text{args}_1 \supset \{\mathcal{Z}_i, \{(\rho_j, y_{(i,j)})_{j=1}^K, \rho_{(max)}, (nMv)\}\}$
  - 9: **else**
  - 10:  $(\mathcal{Z}_i, \{\rho_j\}_{j=1}^K) = G_0(\text{args}_0)$
  - 11:  $\text{args}_0 \supset \{\mathcal{Z}_i, \{(\rho_j, y_{(i,j)})_{j=1}^K, \rho_{(max)}\}\}$
  - ▷ Verification phase
  - 12: **for**  $(s \leftarrow t_{(i,p)}) \geq t^{[th]}$  **do** ▷ Region 3
  - 13: **for all**  $j \in \mathcal{Z}_i$  **do**  $\rho_j \leftarrow \rho_j + u_s \cdot \underline{w}_{(s,j)}$
  - 14: **for all**  $j \in \mathcal{Z}_i$  **do**
  - 15: **if**  $\rho_j > \rho_{(max)}$  **then**  $\rho_{(max)} \leftarrow \rho_j$  and  $a(i) \leftarrow j$
  - 16:  $C_{a(i)}^{[r]} \leftarrow C_{a(i)}^{[r]} \cup \{\hat{\mathbf{x}}_i\}$
- 

by dividing a mean-inverted-index array into two blocks: the first and second blocks consist of moving- and invariant-centroid's tuples, respectively. Figure 6 shows mean-inverted-index arrays  $\xi_s$  with two blocks in Regions 1 and 2 on the left and right sides, where  $(mfM)_s$  denotes the number of moving centroids at the  $s$ th term ID. The arrays in Region 2, in particular, have a double structure due to the two conditions of  $v_{c_{(s,q)}} \geq v^{[th]}$  and that in Eq. (5). If the  $i$ th object satisfies the condition of Eq. (5), we can limit the similarity calculations to only the moving centroids, which are the means of active clusters,  $C_{j \neq a(i)}^{[r-1]} \neq C_{j \neq a(i)}^{[r-2]}$  and only in the first block identified by the top to the  $(mfM)_s$  entries in  $\xi_s$ .

Algorithms 2 and 3 show the pseudocodes of the ES-ICP algorithm and Table III shows the symbols (The complete pseudocodes are in Appendix A). Algorithm 2 differs from MIVI in Algorithm 1 in the following two phases: the gathering phase where the candidate centroids for the similarity

---

### Algorithm 3 Candidate-gathering function: $G_1$

---

**Input:**  $\hat{\mathbf{x}}_i, \check{\mathcal{M}}^{[r-1]}, t^{[th]}, v^{[th]}, \mathcal{Z}_i, \{\rho_j, y_{(i,j)}\}_{j=1}^K, \rho_{(max)}, (nMv)$

▷ (nMv): # moving centroids

**Output:**  $\mathcal{Z}_i, \{\rho_j\}_{j=1}^K$

▷ Exact partial similarity calculation

- 1: **for**  $(s \leftarrow t_{(i,p)}) < t^{[th]}$  in all term IDs in  $\hat{\mathbf{x}}_i$  **do** ▷ Region 1
  - 2: **for**  $1 \leq q \leq (mfM)_s$  **do**
  - 3:  $\rho_{c_{(s,q)}} \leftarrow \rho_{c_{(s,q)}} + u_s \cdot v_{c_{(s,q)}}$
  - 4: **for**  $(s \leftarrow t_{(i,p)}) \geq t^{[th]}$  in all term IDs in  $\hat{\mathbf{x}}_i$  **do** ▷ Region 2
  - 5: **for**  $1 \leq q \leq (mfM)_s$  **do**
  - 6:  $\rho_{c_{(s,q)}} \leftarrow \rho_{c_{(s,q)}} + u_s \cdot v_{c_{(s,q)}}$ ,  
 $y_{(i,c_{(s,q)})} \leftarrow y_{(i,c_{(s,q)})} - u_s$
  - ▷ Upper-bound calculation
  - 7: **for**  $1 \leq j' \leq (nMv)$  **do**
  - 8:  $j'$  is transformed to  $j$ .
  - 9:  $\rho_j^{[ub]} \leftarrow \rho_j + \{y_{(i,j)} \cdot v^{[th]}\}^6$  ▷ Region 3 (UB)
  - ▷ ES filtering
  - 10: **if**  $\rho_j^{[ub]} > \rho_{(max)}$  **then**  $\mathcal{Z}_i \leftarrow \mathcal{Z}_i \cup \{j\}$
- 

calculations of the  $i$ th object are collected in  $\mathcal{Z}_i$  using the ES and ICP filters at lines 6 to 9 and the verification phase where exact similarities for the centroids passing through the filters are calculated at lines 12 to 13 and compared with similarity threshold  $\rho_{(max)}$  at line 15. The two filters effectively prune unnecessary centroids and reduce the multiplications. This decreases the number of instructions, which is one of the performance-degradation factors.

Algorithm 3 shows the  $G_1$  function at line 7 in Algorithm 2. The function works for the  $i$ th object if it is more similar: it calculates upper-bound similarity  $\rho_j^{[ub]}$  in Eq. (4) and returns both the candidate centroid-ID set  $\mathcal{Z}_i$  and the sum of the partial similarities in Regions 1 and 2. Owing to the structured mean-inverted index with the two structural parameters shared in all the objects, the function can avoid using irregular conditional branches for the similarity calculations only by setting loop endpoints at  $(mfM)_s$  in each mean-inverted array. The  $G_0$  function in Algorithm 2 differs from the  $G_1$  in the endpoints in Regions 1 and 2 and the number of centroids for calculating the upper bounds on similarities. Their values in  $G_1$  are  $(mfM)_s, (mfM)_s$ , and  $(nMv)$  while those in  $G_0$  are  $(mf)_s, (mfH)_s$ , and  $K$ . The functions of  $G_1$  and  $G_0$  successfully work in the AFM, i.e., they avoid using irregular conditional branches that induce branch mispredictions and loading unnecessary large arrays that cause cache misses. Thus, our ES-ICP algorithm designed by exploiting the UCs works in the AFM, resulting in high-speed performance.

## V. STRUCTURAL PARAMETERS

To make our ES-ICP more effective, we estimate structural parameters  $t^{[th]}$  and  $v^{[th]}$  depending on the given data set and  $K$  value rather than clamped at predetermined values. Then, we have to perform the estimation in the ES-ICP algorithm with as low computational cost as possible, e.g., much less than that required at the one iteration.

We propose an estimation algorithm for determining the

parameters<sup>7</sup>. Our proposed estimation algorithm minimizes objective function  $J$  of the approximate number of the multiplications for similarity calculations  $\tilde{\phi}$  (derived in Appendix B), which is expressed by

$$(t^{[th]}, v^{[th]}) = \arg \min_{\substack{v_h^{[th]} \in V^{[th]} \\ s_{(min)} \leq s' \leq D}} (J(s', v_h^{[th]})) \quad (6)$$

$$\begin{aligned} J(s', v_h^{[th]}) &= \tilde{\phi}_{(s', h)} \\ &= (\phi 1)_{s'} + (\phi 2)_{(s', h)} + (\tilde{\phi} 3)_{(s', h)}, \end{aligned} \quad (7)$$

where  $s'$  is a candidate of  $t^{[th]}$ ,  $s_{(min)}$  the predetermined minimum value of  $s'$ , and  $v_h^{[th]}$  the  $h$ th candidate of  $v^{[th]}$  that is prepared before ES-ICP starts. The numbers of multiplications in Regions 1 and 2,  $(\phi 1)_{s'}$  and  $(\phi 2)_{(s', h)}$ , are expressed by

$$(\phi 1)_{s'} = \sum_{s=1}^{s'-1} (df)_s \cdot (mf)_s \quad (8)$$

$$(\phi 2)_{(s', h)} = \sum_{s=s'}^D (df)_s \cdot (mfH)_{(s, v_h^{[th]})}, \quad (9)$$

where  $(\phi 1)_{s'} + (\phi 2)_{(s', h)}$  is exactly determined, given the tentative  $s'$  and  $v_h^{[th]}$ . By contrast, it is difficult to exactly determine with low computational cost the number of multiplications in Region 3. To approximate this number so as to compute with low cost, we introduce a probability that a centroid passes through the ES filter, which corresponds to  $|\mathcal{Z}_i|/K$ , and express an approximate number as the expected value  $(\tilde{\phi} 3)_{(s', h)}$ :

$$(\tilde{\phi} 3)_{(s', h)} = \sum_{i=1}^N (ntH)_{(i, s')} \cdot K \cdot \text{Prob}(\rho^{[ub]}(i) \geq \rho_{a(i)}; s', h), \quad (10)$$

where  $(ntH)_{(i, s')}$  is the number of the terms whose IDs are more than or equal to  $s'$ ,  $\rho^{[ub]}(i)$  denotes the distribution function of the upper-bound similarity of the  $i$ th object (Appendix C), and  $\text{Prob}(\rho^{[ub]}(i) \geq \rho_{a(i)}; s', h)$  is the probability of  $\rho^{[ub]}(i) \geq \rho_{a(i)}$ , given  $s'$  and  $h$  (used instead of  $v_h^{[th]}$ ). The probability is represented by

$$\text{Prob}(\rho^{[ub]}(i) \geq \rho_{a(i)}; s', h) = \left(\frac{1}{K}\right) \left(\frac{K}{e}\right)^{\frac{\Delta \bar{\rho}(i; s', h)}{\rho_{a(i)} - \bar{\rho}_i}} \quad (11)$$

$$\Delta \bar{\rho}(i; s', h) = \bar{\rho}^{[ub]}(i; s', h) - \bar{\rho}_i, \quad (12)$$

where  $\bar{\rho}^{[ub]}(i; s', h)$  denotes the average upper bound on the similarities of the  $i$ th object to all the centroids and  $\bar{\rho}_i$  denotes the average similarity to them (derived in Appendix C). Then Eq. (10) is rewritten as

$$(\tilde{\phi} 3)_{(s', h)} = \sum_{i=1}^N (ntH)_{(i, s')} \cdot \left(\frac{K}{e}\right)^{\frac{\Delta \bar{\rho}(i; s', h)}{\rho_{a(i)} - \bar{\rho}_i}}. \quad (13)$$

By substituting Eqs. (8), (9), and (13) into Eq. (7), the objective function is expressed by

$$J(s', v_h^{[th]}) = \sum_{s=1}^{s'-1} (df)_s \cdot (mf)_s + \sum_{s=s'}^D (df)_s (mfH)_{(s, v_h^{[th]})}$$

<sup>7</sup>The estimation algorithm is integrated into the ES-ICP algorithm. Its required elapsed time is merged with the elapsed time spent by the ES-ICP for a fair comparison.

$$+ \sum_{i=1}^N (ntH)_{(i, s')} \cdot \left(\frac{K}{e}\right)^{\frac{\Delta \bar{\rho}(i; s', h)}{\rho_{a(i)} - \bar{\rho}_i}}. \quad (14)$$

We obtain the two structural parameters of  $t^{[th]}$  and  $v^{[th]}$  by efficiently solving Eq. (6) using the objective function in Eq. (14) (detailed in Appendix C).

## VI. EXPERIMENTS

We first describe the data sets and the extracted feature values, followed by a platform for the algorithm evaluation and performance measures. We next compare our ES-ICP with the baseline MIVI and three algorithms, ICP, TA-ICP, and CS-ICP, which were simply extended from existing search and clustering algorithms based on the state-of-the-art techniques in our setting [9], [12], [28], [29]. ICP employs only the auxiliary filter designed so as to operate in the AFM. TA-ICP and CS-ICP incorporate their main UBP filters besides the ICP filter. For its main filter, TA-ICP modifies the threshold algorithms (TA) in the search algorithms in Fagin<sup>+</sup> [28] and Li<sup>+</sup> [12]. CS-ICP utilizes the Cauchy-Schwarz inequality, which is widely used for making upper bounds on an inner product of the vectors [9], [29]. TA-ICP and CS-ICP are described in Section VI-D and detailed in Section F.

### A. Data Sets

We employed two different types of large-scale and high-dimensional sparse real document data sets: *PubMed Abstracts* (PubMed) [42] and *The New York Times Articles* (NYT).

PubMed contains 8 200 000 documents (data objects) each of which was represented by term (distinct word) counts, called 8.2M-sized PubMed. The data set contained terms corresponding to the dimensionality of 141 043. The average number of non-zero elements in the objects was 58.96, and the sparsity indicator ( $\hat{D}/D$ ) (Section I) was  $4.18 \times 10^{-4}$ . By contrast, the average number of non-zero elements in the centroids was 2094.94, which is 35.53 times larger than that in the objects, when  $K = 8 \times 10^4$ . Note that mean-feature vectors are still sparse although they contain more terms than object-feature vectors on average.

Regarding NYT, we extracted 1 285 944 articles (data objects) from *The New York Times Articles* from 1994 to 2006 and counted the occurrence frequencies of the terms after stemming and stop word removal. The number of resultant terms in all the objects was 495 126. The average number of non-zero elements in the objects was 225.76, where  $\hat{D}/D = 4.56 \times 10^{-4}$ . The average number of non-zero elements in the centroids was 5105.73, which is 22.62 times larger than that in the objects when  $K = 1 \times 10^4$ .

We made an object-feature vector from the occurrence frequencies of the terms in the data set. An element of the feature vector was the value of the classic *tf-idf* (term frequency-inverse document frequency), normalized by the  $L_2$ -norm of the feature vector. The *tf-idf* value of the  $s$ th term in the  $i$ th document was defined as

$$tf\text{-idf}(s, i) = tf(s, i) \times \log\left(\frac{N}{(df)_s}\right), \quad (15)$$



where  $tf(s, i)$  denotes the raw counts of the  $s$ th term in the  $i$ th document and  $(df)_s$  denotes the document frequency of the  $s$ th term. Due to normalization, each feature vector was regarded as a point on a unit hypersphere.

### B. Platform and Performance Measures

The algorithms were executed on a computer system that was equipped with two Xeon E5-2697v3 2.6-GHz CPUs with three-level caches from levels 1 to 3 (last level) and 256-GB main memory, by multithreading with OpenMP [49] of 50 threads within the memory capacity. The CPU performed the out-of-order superscalar execution with eight issue widths. The algorithms were implemented in C and compiled with a GNU C compiler version 8.2.0 on the optimization level of `-O3`.

The performances were evaluated with the following measurements: elapsed time until convergence, number of multiplications, performance-degradation factors, and maximum size of the physical memory occupied through the iterations. The accuracy of the clustering results was not our performance measure because the algorithms were just accelerations of the spherical  $K$ -means.

### C. Compared Algorithms

We evaluated our proposed algorithm ES-ICP by comparing it with the baseline algorithm MIVI and three algorithms using state-of-the-art techniques in our setting. The first algorithm only uses the ICP filter, which is referred to as ICP. The second algorithm combined a method inspired by Fagin<sup>+</sup>'s TA [28] and Li<sup>+</sup>'s cosine-threshold algorithm [12] with ICP (TA-ICP). The third algorithm incorporated the Cauchy-Schwarz inequality as in Bottesch<sup>+</sup> [29] or Knittel<sup>+</sup> [9] to ICP (CS-ICP). We briefly describe TA-ICP and CS-ICP (detailed in Appendix F). Both algorithms used the identical framework as ES-ICP for a fair comparison, based on a three-region partition in their mean-inverted indexes and two phases for gathering candidates and their verification. Incorporating parameter  $t^{[th]}$  leads to save the required memory size of  $\mathcal{M}^{p[r]}$  at the verification phase in Section IV-B. The  $t^{[th]}$  was preset at  $0.9D$ , which was close to the value obtained by our estimation algorithm in Section V. TA-ICP and CS-ICP differed from ES-ICP mostly in the following four points:

- 1) main upper-bound-based pruning (UBP) filters
- 2) structures of the partial mean-inverted indexes
- 3) usage of additional partial mean-inverted indexes
- 4) operations in the gathering phase and the exact similarity calculations.

1) *TA-ICP*: TA-ICP employs an individual structural parameter (*threshold*) on the mean-feature values for each object while our algorithm uses the common structural parameter  $v^{[th]}$ , which is shared among all the objects. The individual threshold  $v_{(ta)i}^{[th]}$  for the  $i$ th object is defined by

$$v_{(ta)i}^{[th]} = \rho_{(max)} / \|\mathbf{x}_i\|_1, \quad (16)$$

where  $\rho_{(max)}$  denotes the similarity of the  $i$ th object to the centroid to which the object is assigned at the last iteration and  $\|\mathbf{x}_i\|_1$  the  $L_1$ -norm of the object, i.e.,  $\|\mathbf{x}_i\|_1 = \sum_{p=1}^{(nt)_i} u_{t(i,p)}$ .

Upper bound  $\rho_{(j;i)}^{[ub]}$  on the similarity to the  $j$ th centroid, which is used in the main filter, is expressed by

$$\rho_{(j;i)}^{[ub]} = (\rho 1)_{(j;i)} + (\rho 2')_{(j;i)} + v_{(ta)i}^{[th]} \cdot y_{(i,j)}^8 \quad (17)$$

$$y_{(i,j)} = \sum_{s \geq t^{[th]}} u_{(s,j)}, \quad s = t_{(i,p)}, \quad (18)$$

where  $(\rho 2')_{(j;i)}$  denotes partial similarity in Region 2, determined by  $v_{(ta)i}^{[th]}$ , and  $y_{(i,j)}$  is the partial  $L_1$ -norm of the  $i$ th object-feature vector, which remains unused for  $(\rho 1)_{(j;i)} + (\rho 2')_{(j;i)}$ , and  $u_{(s,j)}$  denotes the object-feature value with the  $s$ th term ID, given the  $j$ th centroid. The upper bound  $\rho_{(j;i)}^{[ub]}$  in Eq. (17) works as the UBP filter, compared with  $\rho_{(max)}$ .

TA-ICP uses a special *partial* mean-inverted index, each array of which is sorted in descending order of mean-feature values, and calculates a part of  $(\rho 2')_{(j;i)}$  while going down in the array from the top to the position of threshold  $v_{(ta)i}^{[th]}$ .

To combine the main filter TA with ICP, an *additional* sorted mean-inverted index only for moving centroids was incorporated because TA-ICP needs a sorted mean-inverted index. For calculating  $(\rho 2')_{(j;i)}$ , the additional sorted mean-inverted index is used if the  $i$ th object is more similar in Eq. (5), otherwise, the sorted mean-inverted index is done.

TA-ICP prepares another partial mean-inverted index for calculating exact similarities of centroids passing through the filters, which corresponds to  $\mathcal{M}^{p[r]}$  in ES-ICP (Table III) but differs in that it has all the mean-feature values due to using the individual threshold  $v_{(ta)i}^{[th]}$ . When calculating the exact similarity, it has to skip with conditional branches the mean-feature values larger than or equal to  $v_{(ta)i}^{[th]}$  that are already being utilized for  $(\rho 2')_{(j;i)}$ .

TA-ICP suffers from the disadvantages of more BMs and LLCMs in Table IV. These are attributed to properties of the TA algorithm itself, that is, finding out a termination point of the gathering phase in its sorted inverted index like Fagin<sup>+</sup> and Li<sup>+</sup>. The BMs were caused by the conditional branches that irregularly return their judgments of whether or not a current point is the termination one. The LLCMs were induced by simultaneously using the three distinct arrays, which were for the partial similarity  $(\rho 1)_{(j;i)} + (\rho 2')_{(j;i)}$ , the partial mean-inverted index, and the additional one.

2) *CS-ICP*: CS-ICP employs upper bound  $\rho_{(j;i)}^{[ub]}$  on the similarity to the  $j$ th centroid based on the Cauchy-Schwarz inequality in Regions 2 and 3, which is expressed by

$$\rho_{(j;i)}^{[ub]} = (\rho 1)_{(j;i)} + \|\mathbf{x}_i^p\|_2 \times \sqrt{\|\boldsymbol{\mu}_{(j;i)}^p\|_2^2} \quad (19)$$

$$\|\mathbf{x}_i^p\|_2 = \sqrt{\sum_{t_{(i,p)} \geq t^{[th]}} u_{t(i,p)}^2} \quad (20)$$

$$\|\boldsymbol{\mu}_{(j;i)}^p\|_2^2 = \sum_{\substack{t_{(i,p)} \geq t^{[th]} \\ s \leftarrow t_{(i,p)}}} v_{c(s,q)}^2, \quad j = c_{(s,q)}, \quad (21)$$

where the second term on the right-hand side in Eq. (19) is the upper bound on the partial similarity in the subspace spanned by the bases of the  $i$ th object's inherent dimensions

<sup>8</sup>To this multiplication, the scaling like that in ES-ICP<sup>6</sup> for reducing multiplications cannot be applied due to using the individual threshold.

TABLE IV  
PERFORMANCE COMPARISON

Algo	Avg Mult	Avg time	Inst	BM	LLCM	Max MEM
MIVI	141.2	16.13	16.53	4.082	10.91	0.4935
ICP	31.52	3.709	4.641	2.905	2.759	0.4955
CS-ICP	1.845	4.404	3.785	3.249	4.956	1.095
TA-ICP	9.656	5.086	2.381	19.31	13.64	1.141

of  $t_{(i,p)} \geq t^{[th]}$ . The UBP filter compares the upper bound  $\rho_{(j;i)}^{[ub]}$  in Eq. (19) with  $\rho_{(max)}$ .

Applying the Cauchy-Schwarz inequality to the subspace requires the  $L_2$ -norms of the mean-feature vectors in the subspace. CS-ICP calculates  $\sqrt{\|\mu_{(j;i)}^p\|_2^2}$  on the fly depending on a given object and multiplies it with  $\|\mathbf{x}_i^p\|_2$  ( $i = 1, 2, \dots, N$ ) that is pre-calculated and stored owing to the preset  $t^{[th]}$ . To avoid the excessive sum of squares calculations of  $\|\mu_{(j;i)}^p\|_2^2$ , CS-ICP prepares an additional partial squared-mean-inverted index each entry of which is a tuple of (mean ID, squared mean-feature value) in Regions 2 and 3 with a computational cost of  $\sum_{s=t^{[th]}}^D (mf)_s$ . We, however, still need to perform the square-root operation with high computational cost.

CS-ICP has the disadvantage of more LLCMs in Table IV. This is caused by simultaneously using the three distinct arrays for calculating an upper bound on the similarity, which are for the partial similarity  $(\rho 1)_{(j;i)}$ , object's partial  $L_1$  norm  $\|\mathbf{x}_i^p\|_2$ , and squared mean-feature values. These are indispensable for the multiply-add operation for the upper-bound calculation.

#### D. Performance Comparison

Figures 7(a) and (b) show the number of multiplications (Mult) for similarity calculations, including their upper-bound calculations, and the complementary pruning rate (CPR) along the iterations until convergence when the algorithms were applied to 8.2M-sized PubMed with  $K = 80\,000$ . The CPR is defined by

$$\text{CPR} = \frac{1}{N} \sum_{i=1}^N \frac{|\mathcal{Z}_i|}{K}, \quad (22)$$

where  $|\mathcal{Z}_i|$  denotes the number of centroids passing through the filter<sup>9</sup>. An algorithm achieving a lower CPR value has better filter function. The Mult and CPR baselines are those of MIVI, whose CPR is 1.0 because it calculates the exact similarities between all the objects and centroids. The effects of the main filters in TA-ICP, CS-ICP, and ES-ICP are evaluated, compared with ICP that reduced both Mult and CPR with increasing the iterations. Figure 8 shows the elapsed time required by each algorithm in the same setting in Fig. 7. Table IV shows the performance rates of the compared algorithms to ES-ICP in a similar format in Table II where Max MEM in the last column is the rate of the maximum memory size through the iterations.

ES-ICP significantly suppressed the elapsed time compared to the others from the early to the last stage in the iterations. As a result, ES-ICP worked over 15 times faster than MIVI

<sup>9</sup> $|\mathcal{Z}_i|$  approximately corresponds to the second term in the right-hand side in Eq. (11).

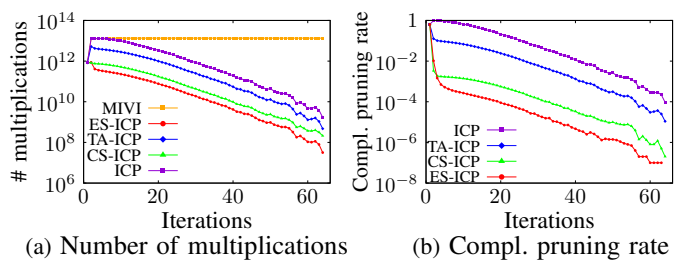


Fig. 7: Algorithm performance in 8.2M-sized PubMed at  $K=80\,000$ : (a) Number of multiplications and (b) Complementary pruning rate (CPR) along iterations until convergence.

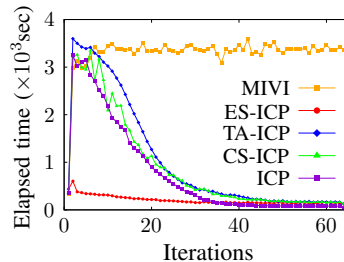


Fig. 8: Elapsed time along iterations until convergence in 8.2M-sized PubMed at  $K=80\,000$

and at least 3.5 times faster than the others. From the values in the three evaluation items of Inst, BM, and LLCM, we know that ES-ICP was designed so as to operate in the AFM. By contrast, TA-ICP and CS-ICP needed more elapsed time than ICP although they had better filters. Their inferior speed-performances are attributed to the difficulty of designing the algorithms in the AFM. Compared with ICP, CS-ICP and TA-ICP caused many last-level-cache load misses (LLCM) because these algorithms needed additional data loaded to the limited-capacity caches. CS-ICP stored the squared mean-feature values in the partial squared-mean-inverted index whose term IDs ( $s$ ) were in the range of  $t^{[th]} \leq s \leq D$ . TA-ICP stored the mean-feature values of the moving centroids in the additional mean-inverted index for all the term IDs. TA-ICP also caused many branch mispredictions (BM) due to the two additional conditional branches for terminating the exact partial similarity calculation in Region 2 and avoiding the double similarity calculations for the centroids passing through its main filter.

Thus, the proposed algorithm ES-ICP achieved higher performance by reducing the performance-degradation factors of Mult, Inst, BM, and LLCM. Regarding the memory usage in Table IV, the three algorithms of ES-ICP, CS-ICP, and TA-ICP needed around double the maximum memory size (Max MEM) of MIVI and ICP since they used partial mean-inverted index  $\mathcal{M}^{[p[r]]}$  for exact similarity calculations for centroids passing through their filters at the verification phase, which is designed so as to work in the AFM. To suppress the maximum memory size, we have to develop new techniques.

## VII. DISCUSSION

We discuss why the ES-ICP algorithm works efficiently from the two viewpoints of the AFM in Section II and the effective use of the UCs of large-scale and high-dimensional

TABLE V  
ALGORITHM CLASSIFICATION

Effective use of UCs	Architecture friendly		
	High	Moderate	Low
Good	ES-ICP	CS-ICP	TA-ICP
Poor	-	ICP	MIVI

sparse document data sets in Section III. First, we classify the algorithms and highlight their characteristics. Next, we describe the efficient operation of our ES filter, relating with both the feature-value-concentration phenomenon and the estimated structural parameter (threshold)  $v^{[th]}$ . Last, we show that ES-ICP efficiently works in the AFM for not only the PubMed but also the NYT data set based on their UCs.

#### A. Algorithm Classification

Regarding these two viewpoints, Table V shows a coarse classification of the algorithms using the mean-inverted index in Sections VI-C. The rows and columns respectively represent the two classes of whether the algorithms effectively used the UCs or not and the three classes of how the algorithms were designed so as to operate in the AFM. Note, however, that all the algorithms are designed to some level in the AFM since they adopt their structured mean-inverted index instead of the data-object-inverted index in Section II.

MIVI is classified into the class where UCs are not used and with a low-level design with respect to the AFM. This is because MIVI without an ICP filter cannot reduce the instructions even at the last stage in the iterations. Furthermore, continuing almost the constant number of the instructions causes that of cache misses to last.

ICP does not effectively use the UCs even though it is designed in a moderate-level AFM. It suppresses the number of instructions from the middle and last stages in the iteration owing to its filter and the number of the branch mispredictions by its structured mean-inverted-index without conditional branches to judge whether or not each centroid is invariant.

ES-ICP, CS-ICP, and TA-ICP effectively utilize the UCs by partitioning the mean-inverted index into three regions in Fig. 5. However, they are classified into the different classes on the AFM for their different main UBP filters. ES-ICP is designed in a high-level AFM. It needs neither additional data nor conditional branches for its main filter, which leverages the common  $v^{[th]}$  shared with all the objects in Section IV. By contrast, since CS-ICP and TA-ICP respectively use their additional data for the squared mean-feature-value arrays and the sorted invariant and moving mean-feature-value arrays, they suffer many cache misses. Moreover, TA-ICP employs individual threshold  $v_{(ta)i}^{[th]}$  for every object in Eq. (16). It needs the additional conditional branch for judging the magnitude relationship between  $v_{(ta)i}^{[th]}$  and a mean-feature value, resulting in increasing the branch mispredictions. For these reasons, CS-ICP and TA-ICP are classified into the moderate- and low-level classes on the AFM.

#### B. ES Filter Using Feature-Value-Concentration Phenomenon

Our ES filter effectively exploits the UCs, in particular, the feature-value-concentration phenomenon to make a tight upper

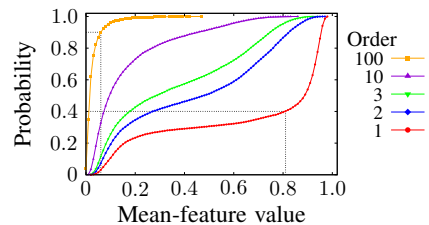


Fig. 9: Probability less than or equal to mean-feature value for orders of 1, 2, 3, 10, 100 in mean-inverted-index arrays sorted in descending order of their values in 8.2M-sized PubMed with  $K=80\,000$

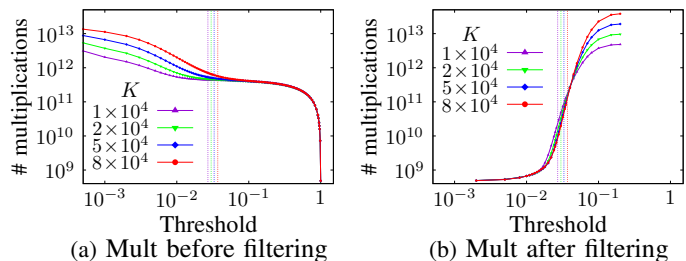


Fig. 10: Number of multiplications: (a) before ES filtering with threshold on horizontal axis and (b) for centroids passing through ES filter when algorithm was applied to 8.2M-sized PubMed. Vertical dashed lines represent actual thresholds.

bound on the similarity with low computational cost. Figure 9 shows the actual skewed form when ES-ICP with  $K = 80\,000$  was applied to 8.2M-sized PubMed. Each curve represents the probability at which a mean-feature value at the order from top to  $(mf)_s$  is less than or equal to the mean-feature value on the horizontal axis. The mean-feature values in Regions 2 and 3 were used, i.e., term IDs ( $s$ ) of the mean-inverted-index arrays satisfied  $t^{[th]} \leq s \leq D$ . In Fig. 9, when the order is 1, the curve represents the probability distribution of the largest feature values in the mean-inverted-index arrays. The probability at a feature value of 0.81 on the first-order curve was only 0.4 while even that at a feature value of 0.06 on the 100th-order curve was 0.9. Considering that the maximum and average order were 75 042 and 10 341, respectively, we know that very few elements in each array have large feature values and most of the remaining have very small values. Based on this characteristic of the feature-value-concentration phenomenon, we can tighten the upper bounds on the similarity by few multiplications in Section IV-A.

From this viewpoint, we confirmed that ES-ICP leverages the skewed form in the mean-inverted-index arrays. Figure 10 shows the number of multiplications (Mult) along threshold (structural parameter)  $v^{[th]}$  when the algorithm with  $t^{[th]} = 1$  was applied to the 8.2M-sized PubMed, where this setting was selected to be independent from our  $t^{[th]}$ . Figure 10(a) depicts the Mult required before filtering, which is the cost for constructing the filter. If  $v^{[th]} = 0$ , Mult corresponds to the number of multiplications required by MIVI, and Mult is zero if  $v^{[th]} = 1$ . The vertical dashed lines represent the actual structural parameters ( $v^{[th]}$ 's) obtained by the estimation algorithm in Section V. Depending on  $K$ , Mult sharply increased in a range less than the threshold. Figure 10(b) depicts Mult, including the zero multiplications, for the centroids passing

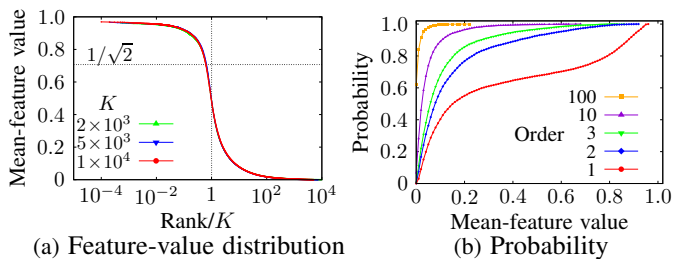


Fig. 11: (a) Skewed form on mean-feature values in 1M-sized NYT data set. (b) Probability less than or equal to mean-feature value in mean-inverted-index arrays sorted in descending order of their values built with  $K=10000$ .

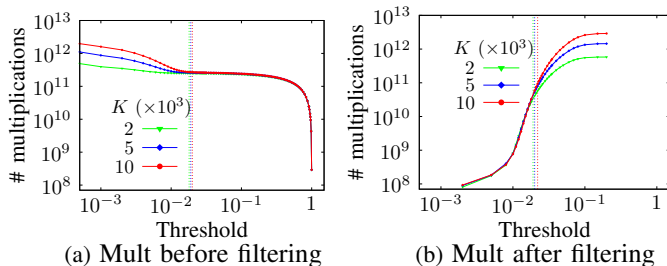


Fig. 12: Number of multiplications: (a) before ES filtering with threshold on horizontal axis and (b) for centroids passing through ES filter when algorithm was applied to 1M-sized NYT. Vertical dashed lines represent actual thresholds.

through the filter. The Mult represents the performance of the constructed filter, where a better filter shows a lower Mult. From both the figures, it is desirable to set the actual threshold at the mean-feature value so that both the Mults are low. The vertical dashed lines represent the actual estimated thresholds. We know that they were set at the desirable values.

### C. ES-ICP as General Algorithm

We show that ES-ICP is a general algorithm for large-scale document data sets by referring to the experimental results in the 1M-sized NYT data set in Section VI-A. Figures 11(a) and (b) respectively show the similar skewed form of the mean-feature values to those in Figs. 4 and 9 in the 8.2M-sized PubMed. That is, each of the many mean-feature vectors had a very large feature value. These results show the feature-value concentration phenomenon and indicate that a cluster is annotated by one or a few dominant terms with very large feature values. Compared with the 8.2M-sized PubMed, the rates of Rank/ $K$  over  $(1/\sqrt{2})$  and the maximum feature values were slightly small, and the probability curves also indicated a similar but slightly different tendency in the mean-feature-value bias. This difference probably stems from both the terminology in the newspaper articles (NYT) and the corpus of the biomedical literature (PubMed) as well as the balance of the dataset size and the amount of vocabulary.

Figures 12(a) and (b) correspond to Figs. 10(a) and (b). The numbers of multiplications required before and after filtering for 1M-sized NYT depicted similar curves to those for the 8.2M-sized PubMed. Table VI shows the performance rates of the compared algorithms to ES-ICP, which corresponds to Table IV. Comparing the two tables, we see similar tendencies

TABLE VI  
PERFORMANCE COMPARISON IN NYT

Algo.	Avg Mult	Avg time	Inst	BM	LLCM	Max MEM
MIVI	81.1	17.2	25.6	1.89	19.8	0.52
ICP	16.4	4.30	5.77	1.38	3.99	0.52
CS-ICP	0.89	5.44	4.88	1.66	13.9	1.06
TA-ICP	12.1	6.80	6.06	10.6	20.0	1.09

despite different data sets. Thus, the proposed algorithm ES-ICP efficiently performed spherical  $K$ -means clustering for large-scale and high-dimensional sparse document data sets.

## VIII. RELATED WORK

This section reviews the algorithms and techniques that are closely related to our proposed algorithm in two distinct topics, Lloyd-type  $K$ -means clustering algorithms and search algorithms with inverted indexes, and describes their drawbacks and availability in our settings.

### A. $K$ -means Clustering Algorithms

Many Lloyd-type acceleration algorithms have been studied for dense object-feature vectors in a metric space [13], [14], [16], [29], [30], [50], [51]. Their key strategies are using lower bounds on distances between an object and centroids for skipping unnecessary distance calculations. Elkan's [14] and Hamerly's algorithms [15] and their variants [17]–[20] are typical examples based on the former key strategy. They leverage the distances calculated at the previous iteration and the moving distances between identical centroids at two consecutive iterations (Appendix J). However, using the moving distance limits the acceleration in the last stage at the iterations where most centroids slightly move or become invariant. Among them, Drake<sup>+</sup> [17] and Ding<sup>+</sup> [18] make the lower bounds tighter using distinct structural parameters proportional to  $K$ . Given a large  $K$  value like in our setting, they need a large amount of memory and are not practical.

Bottesch<sup>+</sup> algorithm [29] uses the Cauchy-Schwarz inequality to obtain the lower bound on a Euclidean distance between data-object- and mean-feature vectors. To tighten the bound, the algorithm partitions a given feature space into disjoint subspaces whose number is an empirical parameter. The algorithm is inefficient if it is naively applied to document data with small values of  $(\hat{D}/D)$ . This is because the set-intersection size of the terms in an object and a centroid is very small, and then the bound by this algorithm is loosened. To avoid such inefficiency, a subspace might be used where an object-feature vector is contained instead of pre-defined subspaces. This approach, however, is also inefficient because of the results of CS-ICP (Section VI-D).

Newling<sup>+</sup> [20] and Xia<sup>+</sup> algorithms [51] structure a centroid set. Exponion in Newling<sup>+</sup> eliminates centroids outside a ball defined for each object from distance-calculation candidates. The ball's center is a centroid of a cluster whose radius is derived based on the triangle inequality. Xia<sup>+</sup> algorithm regards a previous cluster as a ball and narrows down the distance-calculation candidates using a geometric relationship of the balls. A ball's center is a centroid, and its radius

is the distance to the farthest object in the cluster. These algorithms are unsuitable for high-dimensional data sets like document data because they were originally developed for low-dimensional ones. Furthermore, they need to store centroid-centroid distances with  $\mathcal{O}(K^2)$  memory consumption, which is prohibited in our setting where large  $K$  values are used.

Kaukoranta<sup>+</sup> algorithm [13] using its ICP filter deals with a special case where the moving distance is zero. Due to its simplicity, it is used as an auxiliary filter in several algorithms [9], [29], [30], [51]. We also use it because it is easily implemented for an inverted index in the AFM.

### B. Search Algorithms with Inverted Indexes

A threshold algorithm (TA) [28] is a well-known classic algorithm with guaranteed optimality. TA's inverted-index consists of arrays called postings lists each entry of which is sorted in descending order of its feature value. TA collects document ID's in the postings until each of the moving cursors on the postings lists reaches a pre-defined position for a stopping condition of its gathering phase. The strategy needs to execute many conditional branches. If TA is applied to  $K$ -means clustering, it does not always reduce the elapsed time. In fact, the TA-ICP algorithm, inspired by TA in Section VI-D, required more elapsed time than the ICP algorithm without any UBP filter although TA-ICP reduced the multiplications.

A TA-based algorithm [12] was recently reported that utilizes a complete and tight stopping condition and a traversal strategy with a near-optimal access cost over its inverted index. Despite the near-optimal access cost, the algorithm uses many conditional branches like TA and also needs additional computational costs to achieve near-optimality. It does not take into account any negative impacts of the performance-degradation factors. This casts doubts on the algorithm's actual speed-performance.

Fast algorithms in the document-at-a-time (DAAT) query evaluation such as WAND [52]<sup>10</sup> and its variants [53] dynamically skip unnecessary similarity calculations. For the same reason as the TA-based algorithm, they suffer from such tail queries as long queries in our settings although they may achieve an expected performance for short queries. This is attributed to their dynamic skipping techniques, which are far from the operation in the AFM in Section II. Irregularly skipping postings by their conditional branches caused many branch mispredictions and cache misses [54].

## IX. CONCLUSIONS

We proposed the accelerated spherical  $K$ -means clustering algorithm ES-ICP with a large  $K$  value, which is suitable for large-scale and high-dimensional sparse document data sets such as the 8.2M-sized PubMed and 1M-sized NYT data sets. ES-ICP efficiently works with the structured mean-inverted index and the two filters of the novel ES and auxiliary ICP that are designed using the universal characteristics (UCs) of the document data sets so as to operate in the architecture-friendly manner (AFM). We presented the estimation algorithm for the

two structural parameters that partition the structured mean-inverted index into three regions, resulting in a tight upper bound on the similarity between the object- and mean-feature vectors. By using the tight upper bound, the ES filter achieved high pruning rates in all the iterations. We confirmed that ES-ICP performed over 15 times and at least three times faster than the baseline MIVI and the compared algorithms using the state-of-the-art techniques for the 8.2M-sized PubMed, given  $K = 80\,000$ , respectively.

The following issues remain for future work. To extend the ranges of applications and platforms of our proposed algorithm, we will investigate its availability to (1) various data sets and features and (2) computer systems with GPUs.

## REFERENCES

- [1] S. P. Lloyd, "Least squares quantization in PCM," *IEEE Trans. Information Theory*, vol. 28, no. 2, pp. 129–137, 1982.
- [2] J. B. MacQueen, "Some methods for classification and analysis of multivariate observations," in *Proc. 5th Berkeley Symp. Mathematical Statistics and Probability*, 1967, pp. 281–297.
- [3] A. Ng, M. Jordan, and Y. Weiss, "On spectral clustering: Analysis and an algorithm," in *Proc. Advances in Neural Information Processing Systems*, T. Dietterich, S. Becker, and Z. Ghahramani, Eds., vol. 14. MIT Press, 2001.
- [4] U. von Luxburg, "A tutorial on spectral clustering," *Statistics and Computing*, vol. 17, pp. 395–416, December 2007. [Online]. Available: <https://doi.org/10.1007/s11222-007-9033-z>
- [5] J. Wu, Y. Wang, Z. Wu, Z. Wang, A. Veeraraghavan, and Y. Lin, "Deep k-means: Re-training and parameter sharing with harder cluster assignments for compressing deep convolutions," in *Proc. 35th Int. Conf. Machine Learning (ICML)*, J. Dy and A. Krause, Eds., vol. 80. PMLR, 10–15 Jul 2018, pp. 5363–5372. [Online]. Available: <https://proceedings.mlr.press/v80/wu18h.html>
- [6] M. Cho, K. Alizadeh-Vahid, S. Adya, and M. Rastegari, "DKM: Differentiable k-means clustering layer for neural network compression," in *Int. Conf. Learning Representations (ICLR)*, 2022.
- [7] I. S. Dhillon and D. S. Modha, "Concept decompositions for large sparse text data using clustering," *Machine Learning*, vol. 42, no. 1–2, pp. 143–175, 2001. [Online]. Available: <http://doi.org/10.1023/A:1007612920971>
- [8] I. S. Dhillon, J. Fan, and Y. Guan, "Efficient clustering of very large document collections," in *Data Mining for Scientific and Engineering Applications. Massive Computing*, R. L. Grossman, C. Kamath, P. Kegelmeyer, V. Kumar, and R. R. Namburu, Eds. Boston, MA: Springer, 2001, pp. 357–381.
- [9] J. Knittel, S. Koch, and T. Ertl, "Efficient sparse spherical k-means for document clustering," in *Proc. 21st ACM Symp. Document Engineering (DocEng)*, August 2021, pp. 1–4. [Online]. Available: <https://doi.org/10.1145/3469096.3474937>
- [10] Q. Huang, P. Luo, and A. K. H. Tung, "A new sparse data clustering method based on frequent items," *Proc. ACM Manag. Data*, vol. 1, no. 1, p. Article 5, 2023.
- [11] E. Schubert, A. Lang, and G. Feher, "Accelerating spherical k-means," in *SISAP 2021: Similarity Search and Applications*, ser. Lecture Notes in Computer Science. Springer, Cham., 2021, vol. 13058, pp. 217–231. [Online]. Available: [https://doi.org/10.1007/978-3-030-89657-7\\_17](https://doi.org/10.1007/978-3-030-89657-7_17)
- [12] Y. Li, J. Wang, B. Pullman, N. Bandeira, and Y. Papakonstantinou, "Index-based, high-dimensional, cosine threshold querying with optimality guarantees," in *Proc. 22nd Int. Conf. Database Theory (ICDT)*, P. Barcelo and M. Calautti, Eds., no. 11, 2019, pp. 11:1–11:20.
- [13] T. Kaukoranta, P. Fränti, and O. Nevalainen, "A fast exact GLA based on code vector activity detection," *IEEE Trans. Image Process.*, vol. 9, no. 8, pp. 1337–1342, 2000.
- [14] C. Elkan, "Using the triangle inequality to accelerate k-means," in *Proc. 20th Int. Conf. Machine Learning (ICML)*, 2003, pp. 147–153.
- [15] G. Hamerly, "Making k-means even faster," in *Proc. SIAM Int. Conf. Data Mining (SDM)*, 2010, pp. 130–140.
- [16] G. Hamerly and J. Drake, "Accelerating Lloyd's algorithm for k-means clustering," in *Partitional Clustering Algorithms*, M. E. Celebi, Ed. Springer, 2015, ch. 2, pp. 41–78.
- [17] J. Drake and G. Hamerly, "Accelerated k-means with adaptive distance bounds," in *Proc. 5th NIPS Workshop on Optimization for Machine Learning*, 2012.

<sup>10</sup>The original algorithm is heuristic and out of our scope.

- [18] Y. Ding, Y. Zhao, X. Shen, M. Musuvathi, and T. Mytkowicz, “Yinyang k-means: A drop-in replacement of the classic k-means with consistent speedup,” in *Proc. 32nd Int. Conf. Machine Learning (ICML)*, ser. Proc. Machine Learning Research, F. Bach and D. Blei, Eds., vol. 37. Lille, France: PMLR, 07–09 July 2015, pp. 579–587.
- [19] P. Ryšavý and G. Hamerly, “Geometric methods to accelerate k-means algorithms,” in *Proc. SIAM Int. Conf. Data Mining (SDM)*, 2016, pp. 324–332.
- [20] J. Newling and F. Fleuret, “Fast k-means with accurate bounds,” in *Proc. 33rd Int. Conf. Machine Learning (ICML)*, 2016.
- [21] P. Zezula, G. Amato, V. Dohnal, and M. Batko, *Similarity Search: The metric space approach*. Springer, 2006.
- [22] D. Harman, E. Fox, R. Baeza-Yates, and W. Lee, “Inverted files,” in *Information retrieval: Data structures & algorithms*, W. B. Frakes and R. Baeza-Yates, Eds. New Jersey: Prentice Hall, 1992, ch. 3, pp. 28–43.
- [23] D. E. Knuth, “Retrieval on secondary keys,” in *The art of computer programming: Sorting and searching*. Addison-Wesley Professional, 1998, vol. 3, ch. 5.2.4 and 6.5.
- [24] H. Samet, *Foundations of multidimensional and metric data structures*, 1st ed. Morgan Kaufmann, August 2006.
- [25] J. Zobel and A. Moffat, “Inverted files for text search engines,” *ACM Computing Surveys*, vol. 38, no. 2, pp. 1–56, July 2006. [Online]. Available: <https://doi.acm.org/10.1145/1132956.1132959>
- [26] S. Büttcher, C. L. A. Clarke, and G. V. Cormack, *Information retrieval: Implementing and evaluating search engines*. Cambridge, Massachusetts: The MIT Press, 2016.
- [27] K. Aoyama, K. Saito, and T. Ikeda, “Cpi-model-based analysis of sparse k-means clustering algorithms,” *Int. J. Data Sci. Anal.*, vol. 12, pp. 229–248, 2021. [Online]. Available: <https://doi.org/10.1007/s41060-021-00270-4>
- [28] R. Fagin, A. Lotem, and M. Naor, “Optimal aggregation algorithms for middleware,” in *Proc. 20th Symp. Principles of Database Systems (PODS)*. ACM, May 2001, pp. 102–113. [Online]. Available: <https://doi.org/10.1145/375551.375567>
- [29] T. Bottesch, T. Bühler, and M. Kächele, “Speeding up k-means by approximating Euclidean distances via block vectors,” in *Proc. 33rd Int. Conf. Machine Learning (ICML)*, 2016.
- [30] T. Hattori, K. Aoyama, K. Saito, T. Ikeda, and E. Kobayashi, “Pivot-based k-means algorithm for numerous-class data sets,” in *Proc. SIAM Int. Conf. Data Mining (SDM)*, 2016, pp. 333–341.
- [31] A. Z. Broder, L. Garcia-Pueyo, V. Josifovski, S. Vassilvitskii, and S. Venkatesan, “Scalable k-means by ranked retrieval,” in *Proc. 7th ACM Intl. Conf. Web Search and Data Mining (WSDM)*, February 2014, pp. 233–242. [Online]. Available: <http://dx.doi.org/10.1145/2556195.2556260>
- [32] D. Zhang, Y. Cheng, M. Li, Y. Wang, and D. Xu, “Approximation algorithms for spherical k-means problem using local search scheme,” *Theoretical Computer Science*, vol. 853, pp. 65–77, October 2021, special issue on Algorithmic Aspects in Information and Management. [Online]. Available: <https://doi.org/10.1016/j.tcs.2020.06.029>
- [33] D. Arthur and S. Vassilvitskii, “k-means++: The advantages of careful seeding,” in *Proc. 18th annu. ACM-SIAM Symp. Discrete Algorithms (SODA)*, January 2007, pp. 1027–1035.
- [34] B. Bahmani, B. Moseley, A. Vattani, R. Kumar, and S. Vassilvitskii, “Scalable k-means++,” in *Proc. 38th Int. Conf. VLDB Endowment*, August 2012, pp. 622–633.
- [35] M. Li, D. Xu, D. Zhang, and J. Zou, “The seeding algorithms for spherical k-means clustering,” *Journal of Global Optimization*, vol. 76, pp. 695–708, April 2020. [Online]. Available: <https://doi.org/10.1007/s10898-019-00779-w>
- [36] S. Ji, D. Xu, L. Guo, M. Li, and D. Zhang, “The seeding algorithm for spherical k-means clustering with penalties,” *Journal of Combinatorial Optimization*, vol. 44, no. 3, pp. 1977–1994, October 2022.
- [37] J. L. Hennessy and D. A. Patterson, Eds., *Computer architecture, sixth edition: A quantitative approach*. San Mateo, CA: Morgan Kaufmann, 2017.
- [38] Intel Corp., “Intel 64 and ia-32 architectures optimization reference manual,” Jan. 2023. [Online]. Available: <https://software.intel.com/en-us/download/>
- [39] M. Evers and T.-Y. Yeh, “Understanding branches and designing branch predictors for high-performance microprocessors,” *Proc. IEEE*, vol. 89, no. 11, pp. 1610–1620, 2001.
- [40] S. Eyerhan, J. E. Smith, and L. Eeckhout, “Characterizing the branch misprediction penalty,” in *Proc. Int. Symp. Perform. Anal. Syst. Softw. (ISPASS)*, 2006, pp. 48–58.
- [41] M. Fontoura, V. Josifovski, J. Liu, S. Venkatesan, X. Zhu, and J. Zien, “Evaluation strategies for top-k queries over memory-resident inverted indexes,” in *Proc. VLDB Endowment*, 2011.
- [42] D. Dua and E. K. Taniskidou. (2021) Bag of words data set (PubMed abstracts) in UCI machine learning repository. University of California, Irvine, School of Information and Computer Sciences. [Online]. Available: <http://archive.ics.uci.edu/ml>
- [43] Perf, “Linux profiling with performance counters,” 2023. [Online]. Available: <https://perf.wiki.kernel.org>
- [44] L. A. Adamic. (2000) Zipf, power-laws, and Pareto - a ranking tutorial. Information Dynamics Lab, HP Lab. [Online]. Available: <https://www.hpl.hp.com/research/idl/papers/ranking>
- [45] M. E. J. Newman, “Power laws, Pareto distributions and Zipf’s law,” *Contemporary Physics*, vol. 46, no. issue 5, pp. 323–351, 2005. [Online]. Available: <https://doi.org/10.1080/00107510500052444>
- [46] A. Clauset, C. R. Shalizi, and M. E. J. Newman, “Power-law distributions in empirical data,” *SIAM Review*, vol. 51, no. issue 4, pp. 661–703, 2009. [Online]. Available: <https://doi.org/10.1137/070710111>
- [47] M. A. Montemurro, “Beyond the zipf-mandelbrot law in quantitative linguistics,” *Physica A: Statistical Mechanics and its Applications*, vol. 300, no. issue 3–4, pp. 567–578, November 2001. [Online]. Available: [https://doi.org/10.1016/S0378-4371\(01\)00355-7](https://doi.org/10.1016/S0378-4371(01)00355-7)
- [48] J. Z. C. Lai and Y.-C. Liaw, “Improvement of the k-means clustering filtering algorithm,” *Pattern Recognition*, vol. 41, no. 12, pp. 3677–3681, 2008.
- [49] The OpenMP API specification for parallel programming. [Online]. Available: <https://www.openmp.org>
- [50] D. Pelleg and A. W. Moore, “Accelerating exact k-means algorithms with geometric reasoning,” in *Proc. 5th ACM SIGKDD Int. Conf. Knowl. Disc. Data Mining (KDD)*, 1999, pp. 277–281.
- [51] S. Xia, D. Peng, D. Meng, C. Zhang, G. Wang, E. Giem, W. Wei, and Z. Chen, “Ball k-means: Fast adaptive clustering with no bounds,” *IEEE Trans. Pattern Anal. Mach. Intell.*, vol. 44, no. 1, pp. 87–99, 2022.
- [52] A. Z. Broder, D. Carmel, M. Herscovici, A. Soffer, and J. Zien, “Efficient query evaluation using a two-level retrieval process,” in *Proc. 12th Intl. Conf. Information and Knowledge Management (CIKM)*, November 2003, pp. 426–434. [Online]. Available: <https://doi.org/10.1145/956863.956944>
- [53] S. Ding and T. Suel, “Faster top-k document retrieval using block-max indexes,” in *Proc. 34th ACM SIGIR Conf. Research and Development in Information Retrieval (SIGIR)*, July 2011, pp. 993–1002. [Online]. Available: <https://doi.org/10.1145/2009916.2010048>
- [54] M. Crane, J. S. Culpepper, J. Lin, J. Mackenzie, and A. Trotman, “A comparison of document-at-a-time and score-at-a-time query evaluation,” in *Proc. 10th ACM Intl. Conf. Web Search and Data Mining (WSDM)*, February 2017, pp. 201–210. [Online]. Available: <http://dx.doi.org/10.1145/3018661.3018726>

APPENDIX A  
FULL ALGORITHM OF ES-ICP

This section shows in Algorithms 4, 5, and 6 the pseudocode of the full algorithm of ES-ICP in Section IV-B. First, we show the pseudocodes of the assignment step, which correspond to Algorithms 2 and 3. They are rewritten in the form with scaled feature values<sup>6</sup>. The scaling is performed to avoid the multiplications for calculating the upper bounds on similarities. Next, we detail the update step at the  $r$ th iteration in ES-ICP in Algorithm 6, which is not described in Section IV-B.

---

**Algorithm 4** Assignment step in ES-ICP algorithm

---

**Input:**  $\hat{\mathcal{X}}, \check{\mathcal{M}}^{[r-1]}, \check{\mathcal{M}}^{p[r-1]}, \{\rho_{a(i)}^{[r-1]}\}_{i=1}^N, t^{[th]}, v^{[th]}$   
**Output:**  $\mathcal{C}^{[r]} = \{C_j^{[r]}\}_{j=1}^K$   
 $\triangleright$  Scale feature values before assignment step starts  
1: **for all**  $\hat{\mathbf{x}}_i = [(t_{(i,p)}, u_{t_{(i,p)}})]_{p=1}^{(nt)_i} \in \hat{\mathcal{X}}$  **do**  
2:  $u_{t_{(i,p)}} \leftarrow u_{t_{(i,p)}} \cdot v^{[th]}$   $\triangleright$  Scaling  
 $\triangleright$  Calculate similarities in parallel wrt  $\hat{\mathcal{X}}$   
3:  $C_j^{[r]} \leftarrow \emptyset, j = 1, 2, \dots, K$   
4: **for all**  $\hat{\mathbf{x}}_i = [(t_{(i,p)}, u_{t_{(i,p)}})]_{p=1}^{(nt)_i} \in \hat{\mathcal{X}}$  **do**  
5:  $\{\rho_j\}_{j=1}^K \leftarrow 0, \rho_{(max)} \leftarrow \rho_{a(i)}^{[r-1]}, \mathcal{Z}_i \leftarrow \emptyset$   
6: **for**  $j \leftarrow 1$  **to**  $K$  **do**  
7:  $y_{(i,j)} \leftarrow \sum_{t_{(i,p)} \geq t^{[th]}} (u_{t_{(i,p)}})$   $\triangleright$  Initializing  $y_{(i,j)}$   
 $\triangleright$  Gathering phase  
8: **if**  $xState = 1$  **then**  $\triangleright$  ICP filtering  
9:  $(\mathcal{Z}_i, \{\rho_j\}_{j=1}^K) = G_1(\mathcal{Z}_i, \{\rho_j, y_{(i,j)}\}_{j=1}^K, \rho_{(max)}, (nMv))$   
10: **else**  
11:  $(\mathcal{Z}_i, \{\rho_j\}_{j=1}^K) = G_0(\mathcal{Z}_i, \{\rho_j, y_{(i,j)}\}_{j=1}^K, \rho_{(max)})$   
 $\triangleright$  Verification phase  
12: **for**  $(s \leftarrow t_{(i,p)}) \geq t^{[th]}$  **do**  $\triangleright$  Region 3  
13: **for all**  $j \in \mathcal{Z}_i$  **do**  $\rho_j \leftarrow \rho_j + u_s \cdot w_{(s,j)}$   
14: **for all**  $j \in \mathcal{Z}_i$  **do**  
15: **if**  $\rho_j > \rho_{(max)}$  **then**  $\rho_{(max)} \leftarrow \rho_j$  and  $a(i) \leftarrow j$   
16:  $C_{a(i)}^{[r]} \leftarrow C_{a(i)}^{[r]} \cup \{\hat{\mathbf{x}}_i\}$

---



---

**Algorithm 5** Candidate-gathering function:  $G_1$

---

**Input:**  $\hat{\mathbf{x}}_i, \check{\mathcal{M}}^{[r-1]}, t^{[th]}, v^{[th]}, \mathcal{Z}_i, \{\rho_j, y_{(i,j)}\}_{j=1}^K, \rho_{(max)}, (nMv)$   
 $\triangleright$  (nMv): # moving centroids  
**Output:**  $\mathcal{Z}_i, \{\rho_j\}_{j=1}^K$   
 $\triangleright$  Exact partial similarity calculation  
1: **for**  $(s \leftarrow t_{(i,p)}) < t^{[th]}$  in all term IDs in  $\hat{\mathbf{x}}_i$  **do**  $\triangleright$  Region 1  
2: **for**  $1 \leq q \leq (mfM)_s$  **do**  
3:  $\rho_{c_{(s,q)}} \leftarrow \rho_{c_{(s,q)}} + u_s \cdot v_{c_{(s,q)}}$   
4: **for**  $(s \leftarrow t_{(i,p)}) \geq t^{[th]}$  in all term IDs in  $\hat{\mathbf{x}}_i$  **do**  $\triangleright$  Region 2  
5: **for**  $1 \leq q \leq (mfM)_s$  **do**  
6:  $\rho_{c_{(s,q)}} \leftarrow \rho_{c_{(s,q)}} + u_s \cdot v_{c_{(s,q)}}$   
 $y_{(i,c_{(s,q)})} \leftarrow y_{(i,c_{(s,q)})} - u_s$   
 $\triangleright$  Upper-bound calculation  
7: **for**  $1 \leq j' \leq (nMv)$  **do**  
8:  $j'$  is transformed to  $j$ .  
9:  $\rho_j^{[ub]} \leftarrow \rho_j + \boxed{y_{(i,j)}}$   $\triangleright$  Region 3 (UB): Scaling  
 $\triangleright$  ES filtering  
10: **if**  $\rho_j^{[ub]} > \rho_{(max)}$  **then**  $\mathcal{Z}_i \leftarrow \mathcal{Z}_i \cup \{j\}$

---

Algorithm 4 shows the assignment-step pseudocode. Scaling the data-object-feature values at lines 1 to 2 is performed once after the structural parameters  $t^{[th]}$  and  $v^{[th]}$  are determined

---

**Algorithm 6** Update step in ES-ICP algorithm

---

**Input:**  $\hat{\mathcal{X}}, \mathcal{C}^{[r]} = \{C_j^{[r]}\}_{j=1}^K, t^{[th]}$   
**Output:**  $\check{\mathcal{M}}^{[r]}, \check{\mathcal{M}}^{p[r]}, \{\rho_{a(i)}^{[r]}\}_{i=1}^N, [(mfH)_s]_{s=t^{[th]}}^D$   
1: **for all**  $C_j^{[r]} \in \mathcal{C}^{[r]}$  **do**  
 $\triangleright$  (1) Making tentative mean-feature vector  $\lambda$   
2:  $\lambda = (\lambda_s)_{s=1}^D \leftarrow \mathbf{0}$   $\triangleright$  Tentative mean-feature vector  
3: **for all**  $\hat{\mathbf{x}}_i = [(t_{(i,p)}, u_{t_{(i,p)}})]_{p=1}^{(nt)_i} \in C_j^{[r]}$  **do**  
4:  $\lambda_{t_{(i,p)}} \leftarrow \lambda_{t_{(i,p)}} + u_{t_{(i,p)}}$   
5:  $\lambda \leftarrow \lambda / |C_j^{[r]}|, \lambda \leftarrow \boxed{\lambda / (v^{[th]} \cdot \|\lambda\|_2)}$   $\triangleright$  Scaling  
 $\triangleright$  (2) Calculating similarities  $\rho_{a(i)}^{[r]}$   
6: **for all**  $\hat{\mathbf{x}}_i = [(t_{(i,p)}, u_{t_{(i,p)}})]_{p=1}^{(nt)_i} \in C_j^{[r]}$  **do**  
7:  $\rho_{a(i)}^{[r]} \leftarrow \sum_{p=1}^{(nt)_i} u_{t_{(i,p)}} \cdot \lambda_{t_{(i,p)}}$   
 $\triangleright$  (3) Constructing mean-inverted indexes  
8: **for all** term ID  $s$  of  $\lambda_s > 0$  **do**  $\triangleright$  Initialize  $q \leftarrow 1$   
9:  $(c_{(s,q)}, v_{c_{(s,q)}}) \in \xi_s^{[r]} \subset \check{\mathcal{M}}^{[r]} \leftarrow (j, \lambda_s)$   $\triangleright q++$   
10: **if**  $s \geq t^{[th]}$  and  $\lambda_s < v^{[th]}$  **then**  
11:  $w_{(s,j)} (\in \xi_s^{[r]} \subset \check{\mathcal{M}}^{p[r]}) \leftarrow \lambda_s$   
 $\triangleright$  (4) and (5) Structuring  $\xi_s^{[r]} \in \check{\mathcal{M}}^{[r]}$   
12: **for all**  $[\xi_s^{[r]}]_{s=1}^{t^{[th]}-1} \subset \check{\mathcal{M}}^{[r]}$  **do**  
13: Divide  $[(c_{(s,q)}, v_{c_{(s,q)}})]_{q=1}^{(mf)_s}$  into two blocks:  
 $[(c_{(s,q)}, v_{c_{(s,q)}})]_{q=1}^{(mfM)_s}$  and  $[(c_{(s,q)}, v_{c_{(s,q)}})]_{q=(mfM)_s+1}^{(mf)_s}$   
14: **for all**  $[\xi_s^{[r]}]_{s=t^{[th]}}^D \subset \check{\mathcal{M}}^{[r]}$  **do**  
15: Pick up tuples from  $[(c_{(s,q)}, v_{c_{(s,q)}})]_{q=1}^{(mf)_s} \in \xi_s^{[r]}$   
that satisfy  $v_{c_{(s,q)}} \geq v^{[th]}$  and  
make  $[(c_{(s,q)}, v_{c_{(s,q)}})]_{q=1}^{(mfH)_s}$  from them.  
16: Divide  $[(c_{(s,q)}, v_{c_{(s,q)}})]_{q=1}^{(mfH)_s}$  into two blocks:  
 $[(c_{(s,q)}, v_{c_{(s,q)}})]_{q=1}^{(mfM)_s}$  and  $[(c_{(s,q)}, v_{c_{(s,q)}})]_{q=(mfM)_s+1}^{(mfH)_s}$   
 $\triangleright$  Estimating structural parameters (Appendices B and C)  
17: **if**  $r \in \{1, 2\}$  **then**  
18:  $(t^{[th]}, v^{[th]}) \leftarrow EstParams(\check{\mathcal{M}}^{[r]}, \hat{\mathcal{X}}, \text{other arguments})$   
(detailed in Appendix C)  
19: Reconstruct  $\check{\mathcal{M}}^{[r]}$  using new  $(t^{[th]}, v^{[th]})$

---

in the ES-ICP algorithm. Algorithm 5 shows  $G_1$  function in Algorithm 4. Owing to scaling the data-object-feature values in Algorithm 4 and mean-feature values at line 5 in Algorithm 6 (appearing later), we can obtain the upper bound on similarities by only the addition at line 9 without any multiplications in Algorithm 5.

Algorithm 6 shows the pseudocode of the update step at the  $r$ th iteration. The algorithm performs the following five processes at lines 1 to 16.

- 1) Making tentative mean-feature vector  $\lambda$  of the cluster  $C_j^{[r]}$  at lines 2 to 5. In particular, at line 5, scaling the mean-feature values by  $1/v^{[th]}$  is performed. The  $\lambda$  with full expression consists of  $D$  feature values  $\lambda_s$  ( $s = 1, 2, \dots, D$ ).
- 2) Calculating the similarity  $\rho_{a(i)}^{[r]}$  of the  $i$ th object to the centroid of cluster  $C_j^{[r]}$  to which the object belongs at lines 6 and 7. The  $\rho_{a(i)}^{[r]}$  is utilized as the similarity threshold in the gathering phase at the assignment step at the next ( $r+1$ ) iteration, which is for determining whether

the  $i$ th object satisfies the condition of  $\rho_j^{[ub]} > \rho_{(max)}$  ( $\rho_{(max)} \leftarrow \rho_{a(i)}^{[r]}$  at the initialization) for the ES filter, e.g., at line 10 in Algorithm 5.

- 3) Constructing mean-inverted index  $\check{\mathcal{M}}^{[r]}$  and partial mean-inverted index  $\check{\mathcal{M}}^{p[r]}$  using the obtained  $\lambda$  at lines 8 to 11.  $\check{\mathcal{M}}^{p[r]}$ , whose element is  $w_{(s,j)}$ , is utilized for exact similarity calculations in Region 3 at the assignment step in Algorithm 4.  $\check{\mathcal{M}}^{p[r]}$  consists of  $(D - t^{[th]} + 1)$  inverted-index arrays  $\check{\zeta}_s^{[r]}$  whose lengths are  $K$ . The  $j$ th element in  $\check{\zeta}_s$  is mean-feature values  $w_{(s,j)}$  if  $w_{(s,j)} < v^{[th]}$ , otherwise 0. Due to this full expression, the  $j$ th element can be directly accessed by using the centroid ID  $j$  as the key.
- 4) Structuring inverted-index arrays for the ES filter, which are  $\check{\xi}_s^{[r]} \in \check{\mathcal{M}}^{[r]}$  ( $t^{[th]} \leq s \leq D$ ) at lines 14 to 15. Since mean-feature values of  $v_{c(s,q)} \geq v^{[th]}$  are used for calculating exact partial similarities in Region 2, the tuples containing such values are placed from the top of  $\check{\xi}_s^{[r]}$  to the  $(mfH)_s$ th entry.
- 5) Structuring inverted-index arrays  $\check{\xi}_s^{[r]}$  for the ICP filter at lines 12 to 13 in Region 1 and at line 16 in Region 2.

Furthermore, at the first and second iterations, two structural parameters  $t^{[th]}$  and  $v^{[th]}$  are estimated by using *EstParams* function in Algorithm 7 (appearing later) and described in Appendices B and C.  $\check{\mathcal{M}}^{p[r]}$  is constructed after the structural-parameter estimation and then  $\check{\mathcal{M}}^{[r]}$  is updated.

## APPENDIX B

### OBJECTIVE FUNCTION IN SECTION V

The objective function is expressed by Eq. (14) in Section V. Its key term is the probability that the upper bound  $\rho^{[ub]}(i)$  is more than or equal to the similarity threshold  $\rho_{a(i)}$ , given structural-parameter values of  $v_h^{[th]}$  and  $s'$  for  $t^{[th]}$ . To deal with the discrete similarities  $\rho_j$  ( $j = 1, \dots, K$ ) of  $\mathbf{x}_i$  to the  $j$ th centroid, with a continuous relaxation, we introduce the probability density function of  $\rho$ ,  $f(\rho)$ , as the similarity distribution w.r.t.  $\rho$ . Then, we derive the probability of  $\text{Prob}(\rho^{[ub]}(i) \geq \rho_{a(i)}; s', h)$  in Eq. (11) where  $s'$  denotes a candidate of  $t^{[th]}$  and  $h$  represents  $v_h^{[th]}$  that is the  $h$ th candidate of  $v^{[th]}$ . To do this, we assume the following three.

- 1) The probability density function  $f(\rho)$  is approximated by a distribution function in an exponential family:

$$\begin{aligned} f(\rho) &= \lambda_0 \cdot e^{-\lambda_0(\rho - \bar{\rho}_i)} \\ (1/\lambda_0) &= \bar{\rho}_i, \end{aligned} \quad (23)$$

where  $\bar{\rho}_i$  denotes the average of similarities of  $\mathbf{x}_i$  to all the centroids. We apply the condition of  $\rho \geq \bar{\rho}_i$  to  $f(\rho)$ . Then, the following equation holds:

$$\text{Prob}(\rho \geq \bar{\rho}_i) = \int_{\bar{\rho}_i}^{\infty} f(\rho) d\rho = \frac{1}{e}. \quad (24)$$

- 2) We precisely model a probability density function of  $f(\rho, \rho \geq \bar{\rho}_i)$  in the range of  $\rho \geq \bar{\rho}_i$  through the following expression:

$$f(\rho, \rho \geq \bar{\rho}_i) = \text{Prob}(\rho \geq \bar{\rho}_i) \cdot f(\rho | \rho \geq \bar{\rho}_i) \quad (25)$$

$$f(\rho | \rho \geq \bar{\rho}_i) = \lambda \cdot e^{-\lambda(\rho - \bar{\rho}_i)}, \quad (26)$$

where  $(1/\lambda)$  denotes the expected value of  $f(\rho, \rho \geq \bar{\rho}_i)$  and  $\lambda \neq \lambda_0$ .

- 3) Similarity-upper-bound distribution  $f^{[ub]}(\rho, \rho \geq \bar{\rho}_i)$  is expressed by the parallel translation of  $f(\rho, \rho \geq \bar{\rho}_i)$  by  $\Delta\bar{\rho}(i; s', h)$  as

$$\begin{aligned} f^{[ub]}(\rho - \Delta\bar{\rho}(i; s', h), \rho \geq \bar{\rho}_i) &= f(\rho, \rho \geq \bar{\rho}_i) \\ \Delta\bar{\rho}(i; s', h) &= \bar{\rho}^{[ub]}(i; s', h) - \bar{\rho}_i, \end{aligned} \quad (27)$$

where the second equation is the same as Eq. (12).

Since an object belongs to a distinct cluster, i.e., hard clustering, the centroid with a similarity more than or equal to  $\rho_{a(i)}$  is only one of the cluster to which the object belongs. Then, the following equation holds:

$$\begin{aligned} \text{Prob}(\rho > \rho_{a(i)}) &= \int_{\rho_{a(i)}}^{\infty} f(\rho, \rho \geq \bar{\rho}_i) d\rho \\ &= \text{Prob}(\rho \geq \bar{\rho}_i) \cdot e^{-\lambda(\rho_{a(i)} - \bar{\rho}_i)} \\ &= \frac{1}{K}, \end{aligned} \quad (28)$$

where  $\rho_{a(i)}$  denotes the similarity of the  $i$ th object to the centroid of the cluster which the object belongs to. For simplicity, the superscript of  $[r]$  for  $\rho_{a(i)}^{[r]}$ , which represents the  $r$ th iteration, is omitted. Using Eqs. (25), (26), and (28),  $\lambda$  is expressed as

$$\lambda = \frac{\log(K/e)}{\rho_{a(i)} - \bar{\rho}_i}. \quad (29)$$

The probability in Eqs. (10) and (11) is expressed by

$$\begin{aligned} \text{Prob}(\rho^{[ub]}(i) \geq \rho_{a(i)}; s', h) &= \int_{\rho_{a(i)} - \Delta\bar{\rho}(i; s', h)}^{\infty} f(\rho, \rho \geq \bar{\rho}_i) d\rho \\ &= \left(\frac{1}{K}\right) \left(\frac{K}{e}\right)^{\frac{\Delta\bar{\rho}(i; s', h)}{\rho_{a(i)} - \bar{\rho}_i}}. \end{aligned} \quad (30)$$

Then, the expected value of the partial-similarity upper bound in Region 3 in Eq. (10) is rewritten as

$$(\check{\varphi}3)_{(s', h)} = \sum_{i=1}^N (ntH)_{(i; s')} \cdot \left(\frac{K}{e}\right)^{\frac{\Delta\bar{\rho}(i; s', h)}{\rho_{a(i)} - \bar{\rho}_i}}. \quad (31)$$

$\Delta\bar{\rho}(i; s', h)$  is obtained by substituting  $\bar{\rho}_i$  and  $\bar{\rho}^{[ub]}(i; s', h)$  in Eqs. (32) and (33) into Eq. (27).

$$\bar{\rho}_i = \sum_{p=1}^{(nt)_i} \left( u_{t(i,p)} \cdot \frac{1}{K} \sum_{q=1}^{(mf)_s} v_{c(s,q)} \right), \quad s = t(i,p), \quad (32)$$

where  $t_{(i,p)}$  and  $c_{(s,q)}$  respectively denote the term ID appeared at the  $p$ th position in  $\hat{\mathbf{x}}_i$  and the mean ID (cluster ID)



appeared at the  $q$ th position in the inverted-index-array with the  $s$ th term ID  $\xi_s$  (see Table I).

$$\begin{aligned} \bar{\rho}^{[ub]}(i; s', h) &= \sum_{s=1}^{s'-1} \left( u_s \cdot \frac{1}{K} \sum_{q=1}^{(mf)_s} v_{c(s,q)} \right) \\ &+ \sum_{s=s'}^D u_s \cdot \frac{1}{K} \left( \sum_{q=1}^{(mfH)_s} v_{c(s,q)} + v_h^{[th]} \cdot (mfL)_s \right) \end{aligned} \quad (33)$$

where  $(mfL)_s = (mf)_s - (mfH)_{(s, v_h^{[th]})}$  and  $u_s$  is  $u_{t(i,p)}$  if  $u_{t(i,p)}$  exists for  $t(i,p) \geq t^{[th]}$ , 0 otherwise.

We can obtain the objective function by substituting Eqs. (8), (9), and (13) into Eq. (7) as

$$\begin{aligned} J(s', v_h^{[th]}) &= \sum_{s=1}^{s'-1} (df)_s \cdot (mf)_s \\ &+ \sum_{s=s'}^D (df)_s \cdot (mfH)_{(s, v_h^{[th]})} \\ &+ \sum_{i=1}^N (ntH)_{(i, s')} \cdot \left( \frac{K}{e} \right)^{\frac{\Delta \bar{\rho}(i; s', h)}{\rho_{\alpha(i)} - \bar{\rho}_i}}. \end{aligned}$$

### APPENDIX C PARAMETER ESTIMATION IN SECTION V

This section describes our proposed efficient and practical algorithm for simultaneously estimating  $t^{[th]}$  and  $v^{[th]}$ . For the parameter estimation, we suppose that an appropriate  $t^{[th]}$  exists near  $D$  on the grounds of the universal characteristics (UCs) in Section III, i.e., the skewed forms of both the document frequency ( $df$ ) and mean frequency ( $mf$ ) with respect to term ID sorted in ascending order of  $df$  in Figs. 2 and 3, and  $v^{[th]}$  exists in the short range from the top of each inverted-index array  $\xi_s$  due to the skewed form of the mean-feature-values in the array. This allows us to narrow down a search space for the two parameters.

The estimation algorithm minimizes the objective function in Eq. (7) that is rewritten as

$$\begin{aligned} (t^{[th]}, v^{[th]}) &= \arg \min_{\substack{v_h^{[th]} \in V^{[th]} \\ s_{(min)} \leq s' \leq D}} \left( J(s', v_h^{[th]}) \right) \\ J(s', v_h^{[th]}) &= \tilde{\phi}_{(s', h)} = (\phi 1)_{s'} + (\phi 2)_{(s', h)} + (\tilde{\phi} 3)_{(s', h)}, \end{aligned}$$

where  $s'$  denotes the term ID that is a candidate of  $t^{[th]}$  and decremented one by one from  $D$  to the pre-determined minimum term ID of  $s_{(min)}$  and  $h$  represents the  $h$ th candidate of  $v^{[th]}$ , i.e.,  $v_h^{[th]}$ . Based on the presumption that  $t^{[th]}$  exists near  $D$ , the estimation algorithm efficiently calculates  $\tilde{\phi}_{(s', h)}$  for each  $v_h^{[th]}$ <sup>11</sup> by exploiting a recurrence relation with respect

to  $s'$  expressed by

$$\begin{aligned} \tilde{\phi}_{(s'; h)} &= \tilde{\phi}_{(s'+1; h)} - (df)_{s'} \cdot (mfL)_{(s'; v_h^{[th]})} \\ &\quad + (\tilde{\phi} 3)_{(s'; h)} - (\tilde{\phi} 3)_{(s'+1; h)} \quad (34) \\ \tilde{\phi}_{(D+1; h)} &= \sum_{s=1}^D (df)_s \cdot (mf)_s = \phi \\ (\tilde{\phi} 3)_{(D+1; h)} &= 0, \end{aligned}$$

where  $(mfL)_{(s'; v_h^{[th]})} = (mf)_{s'} - (mfH)_{(s'; v_h^{[th]})}$ , i.e.,  $(mfL)_{(s'; v_h^{[th]})}$  denotes the number of centroids whose feature values are lower than  $v_h^{[th]}$ .

Moreover,  $(\tilde{\phi} 3)_{(s'; h)}$  itself in Eq. (34) is represented with a recurrence relation. We rewrite the approximate number of multiplications with respect to the  $i$ th object in Eq. (13) as

$$(\tilde{\phi} 3)_{(i, s'; h)} = (ntH)_{(i, s')} \cdot \left( \frac{K}{e} \right)^{\frac{\bar{\rho}^{[ub]}(i, s'; h) - \bar{\rho}_i}{\rho_{\alpha(i)} - \bar{\rho}_i}}. \quad (35)$$

We consider two cases of the  $i$ th object contains the term whose ID is  $s'$ , i.e.,  $s' \in \{t(i, p)\}_{p=1}^{(nt)_i}$ , and the other. In the latter case,  $(\tilde{\phi} 3)_{(i, s'; h)}$  is invariant from  $(\tilde{\phi} 3)_{(i, s'+1; h)}$  as

$$(\tilde{\phi} 3)_{(i, s'; h)} = (\tilde{\phi} 3)_{(i, s'+1; h)}. \quad (36)$$

In the former case, we derive the recurrence relation while focusing on  $(ntH)_{(i, s')}$  and  $\bar{\rho}^{[ub]}(i, s'; h)$  in Eq. 35. First, the following equation with respect to  $(ntH)_{(i, s')}$  holds:

$$(ntH)_{(i, s')} = (ntH)_{(i, s'+1)} + 1. \quad (37)$$

Next,  $\bar{\rho}^{[ub]}(i, s'; h)$  is expressed by

$$\bar{\rho}^{[ub]}(i, s') = \bar{\rho}^{[ub]}(i, s'+1) + \Delta \bar{v}_{(i, s')} \cdot u_{s'} \quad (38)$$

$$\begin{aligned} \Delta \bar{v}_{(i, s')} &= \frac{1}{K} \sum_{q=(mfH)_{s'}+1}^{(mf)_{s'}} (v_h^{[th]} - v_{c(s,q)}) \\ &\quad + \left( 1 - \frac{(mf)_{s'}}{K} \right) v_h^{[th]}, \end{aligned} \quad (39)$$

where  $u_{s'}$  denotes  $u_{t(i, p)=s'}$  and  $\Delta \bar{v}_{(i, s')}$  is the average difference between  $v_h^{[th]}$  and the exact mean-feature values in Region 3 at the  $s'$ th term ID and  $h$  is omitted for simplicity. Then,  $\bar{\rho}^{[ub]}(i, s'; h)$  is expressed by

$$(\tilde{\phi} 3)_{(i, s'; h)} = (ntH)_{(i, s')} \cdot \left( \frac{K}{e} \right)^{\frac{\bar{\rho}^{[ub]}(i, s'; h) - \bar{\rho}_i}{\rho_{\alpha(i)} - \bar{\rho}_i}} \quad (40)$$

$$(\tilde{\phi} 3)_{(i, s'; h)} = \left( \frac{K}{e} \right)^{\gamma(i, s')} \quad (41)$$

$$\times \left\{ (\tilde{\phi} 3)_{(i, s'+1; h)} + \left( \frac{K}{e} \right)^{\frac{\bar{\rho}^{[ub]}(i, s'+1) - \bar{\rho}_i}{\rho_{\alpha(i)} - \bar{\rho}_i}} \right\} \quad (42)$$

$$\gamma(i, s') = \frac{\Delta \bar{v}_{(i, s')} \cdot u_{s'}}{\rho_{\alpha(i)} - \bar{\rho}_i}, \quad (43)$$

<sup>11</sup>This process for each  $v_h^{[th]}$  is executed in parallel processing.

---

**Algorithm 7** Parameter-estimation function: *EstParams*


---

**Input:**  $\check{\mathcal{M}}, \check{\mathcal{X}}, \check{\mathcal{X}}^p, V^{[th]} = \{v_1^{[th]}, \dots, v_{|V^{[th]|}}^{[th]}\}, s_{(min)}$

**Output:**  $(t^{[th]}, v_h^{[th]})$

▷ Initialization

- 1:  $\phi = \sum_{s=1}^D (df)_s \cdot (mf)_s$
- 2: **for all**  $\hat{x}_i \in \check{\mathcal{X}}$  **do**
- 3:  $\bar{\rho}_i \leftarrow (1/K) \sum_{p=1}^{(ntH)_i} \sum_{q=1}^{(mf)_{s=t(i,p)}} (v_{c(s,q)} \cdot u_{t(i,p)})$

▷ Parallel processing

- 4: **for all**  $v_h^{[th]} \in V^{[th]}$  **do**
- 5:  $\tilde{\phi}_{(D+1,h)} \leftarrow \phi$
- 6:  $(ntH)_{(i,D+1)} \leftarrow 0, \Delta v_{(i,D+1)} \leftarrow 0$  for  $1 \leq i \leq N$
- 7: **for**  $s' \leftarrow D$  **to**  $s_{(min)}$  **do** ▷  $s': t^{[th]}$  candidate
- 8: **for all**  $i = o_{(s',q')} \in \check{\eta}_{s'} \subset \check{\mathcal{X}}^p$  **do**
- 9:  $\tilde{\phi}_{(s',h)} \leftarrow \tilde{\phi}_{(s'+1,h)} - (ntH)_{(i,s'+1)} (K/e)^{\gamma(i,s'+1)}$
- 10:  $\Delta v_{(i,s')} \leftarrow \Delta v_{(i,s'+1)} + \sum_{q=(mfH)'_s+1}^{(mf)_{s'}} (v_h^{[th]} - v_{c(s',q)}) + (K - (mf)_{s'}) \cdot v_h^{[th]}$
- 11:  $\Delta \bar{v}_{(i,s')} \leftarrow \Delta v_{(i,s')}/K$
- 12:  $\gamma_{(i,s')} \leftarrow (\Delta \bar{v}_{(i,s')} \cdot \check{u}_i) / (\rho_{\alpha(i)} - \bar{\rho}_i)$
- 13:  $\tilde{\phi}_{(s',h)} \leftarrow \tilde{\phi}_{(s',h)} + (ntH)_{(i,s')} (K/e)^{\gamma(i,s')}$
- 14:  $\tilde{\phi}_{(s',h)} \leftarrow \tilde{\phi}_{(s',h)} - (df)_{s'} \cdot (mfL)_{(s';v_h^{[th]})}$
- 15:  $J(s', v_h^{[th]}) = \tilde{\phi}_{(s',h)}$
- 16:  $(t_h^{[th]}, v_h^{[th]}) \leftarrow \arg \min_{s_{(min)} \leq s' \leq D} (J(s', v_h^{[th]}))$
- 17:  $(t^{[th]}, v^{[th]}) \leftarrow \arg \min_{1 \leq h \leq |V^{[th]|} } (J(t_h^{[th]}, v_h^{[th]}))$

---

TABLE VII  
NOTATION FOR *EstParams* FUNCTION

Symbol	Description and Definitions
$J(s', v_h^{[th]})$	Function that returns the approximation number of the multiplications $s'$ : Term ID as $t^{[th]}$ candidate $v_h^{[th]}$ : Mean-feature-value as $v^{[th]}$ candidate $v_h^{[th]}$ can be represented with $h$ .
$V^{[th]}$	Set of $v_h^{[th]}, h = 1, \dots,  V^{[th]} $
$(\tilde{\phi})_{(s',h)}$	Approximate number of multiplications for similarity calculations, given $s'$ and $h$
$(df)_s$	Document frequency of $s$ th term ID
$(mf)_s$	Mean frequency of $s$ th term ID
$s_{(min)}$	Minimum term ID of candidates ( $s'$ ) of $t^{[th]}$ , $s_{(min)} \leq s' \leq D$
$\check{\mathcal{X}}^p$	Partial inverted-index of objects, whose column is object-tuple array $\check{\eta}_s, s \geq s_{(min)}$ $\check{\eta}_s = [(o_{(s,q')}, \check{u}_{o_{(s,q')}})]_{q'=1}^{(df)_s}$ $o_{(s,q')}$ : $q'$ th object ID appeared in $\check{\eta}_s$ $\check{u}_{o_{(s,q')}}$ : $q'$ th feature value appeared in $\check{\eta}_s$ $(df)_s$ : Document frequency of $s$ th term ID
$\bar{\rho}_i$	Average similarity of $i$ th object to centroids
$(ntH)_{(i,t^{[th]})}$	Number of terms in $i$ th object whose ID is higher than or equal to given $t^{[th]}$
$(mfH)_{(s';v_h^{[th]})}$	Mean frequency of $s$ th term ID where $v_{(s,q)} \geq v_h^{[th]}$ , given $v_h^{[th]}$ , where $q$ is a position in $\xi_s$
$(mfL)_{(s';v_h^{[th]})}$	$(mfL)_{(s';v_h^{[th]})} = (mf)_s - (mfH)_{(s';v_h^{[th]})}$

where the values in the square bracket are already obtained at the  $(s'+1)$ th term ID. The boundary conditions are set as

$$(\tilde{\phi}3)_{(i,D+1;h)} = 0 \quad (44)$$

$$(ntH)_{(i,D+1)} = 0 \quad (45)$$

$$\bar{\rho}^{[ub]}(i, D+1) = \bar{\rho}_i. \quad (46)$$

By applying Eqs. (36) and (42) to Eq. (34), we can make the recurrence relation.

When using the recurrence relation, we need to access a data-object- and a mean-feature value at the  $s$ th term ID. Although the mean-feature value is easily accessed through the mean-inverted-index array  $\xi_s$  in the inverted index  $\check{\mathcal{M}}$ , it is difficult to selectively access only the data-object feature value at the  $s$ th term ID through the current data-object structure of  $\check{\mathcal{X}}$  at low computational cost. To overcome the difficulty in the architecture-friendly manner (AFM) in Section 2, we introduce a partial object-inverted-index  $\check{\mathcal{X}}^p$  for the term IDs from  $s_{(min)}$  to  $D$  with low memory consumption. By using the partial object-inverted-index, we can access both the feature values at the  $s$ th term ID without using conditional branches causing many mispredictions or loading the large array of the object data set, resulting in efficiently calculating  $(\tilde{\phi}3)_{(i,s';h)}$ .

Algorithm 7 and Table VII show a pseudocode of the practical algorithm *EstParams* and its notation, respectively. Given the  $v^{[th]}$  candidate  $v_h^{[th]} \in V^{[th]}$ , at lines 4 to 16, the tuple of  $(t_h^{[th]}, v_h^{[th]})$  is obtained for each  $v_h^{[th]}$ , where  $t_h^{[th]}$  denotes the  $s'$  that minimizes  $J(s', v_h^{[th]})$ . At line 17,  $(t^{[th]}, v^{[th]})$  is determined as the tuple that minimizes  $J(t_h^{[th]}, v_h^{[th]})$  among all the tuples. At lines 7 to 15, the recurrent relation is used with

the initial state of  $s' = D$ . By using the inverted-index-array  $\check{\eta}_{s'}$  in the data-object inverted index  $\check{\mathcal{X}}^p$ , we can efficiently access the object-feature value  $\check{u}_i$  having the term ID of  $s'$  and calculate the approximate number of the multiplications  $\tilde{\phi}_{(s',h)}$  at lines 8 to 15.

To confirm the effectiveness of the parameter-estimation algorithm *EstParams* in Algorithm 7, we incorporated it to our proposed  $K$ -means clustering algorithm ES-ICP in Section IV and applied ES-ICP with  $K = 80\,000$  to the 8.2M-sized PubMed data set in Section VI. We executed *EstParams* twice, at the first and the second iteration, in ES-ICP. The purpose of its execution at the first iteration is only to reduce the elapsed time in the second iteration. The clustering result at the first iteration strongly depends on its initial setting and some centroids often change their positions significantly. At the second iteration, *EstParams* determines the parameter values that are utilized at the successive iterations.

We compared the approximate number of the multiplications obtained by *EstParams* with the corresponding actual number calculated by ES-ICP, where  $t^{[th]}$  and  $v^{[th]}$  were set at the values estimated at the second iteration. Figure 13 shows the comparison with the approximate and actual number of the multiplications along  $v_h^{[th]}$  at which  $t_h^{[th]}$  at line 16 in Algorithm 7 was a different value in most of the  $v_h^{[th]}$  ranges except in the several small  $v_h^{[th]}$  values. The parameters in *EstParams* were set as  $s_{(min)} = 1.22 \times 10^5$  and  $0.020 \leq v_h^{[th]} \leq 0.060$  by 0.001 step. We observed that the approximate number of the multiplications agreed with the actual number in all the range and each value of  $v_h^{[th]}$ . The minimum number of the

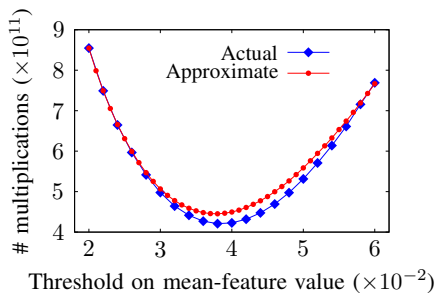


Fig. 13: Comparison of the approximate and actual number of the multiplications along threshold  $v_h^{[th]}$  on the mean-feature value for 8.2M-sized PubMed with  $K=80\,000$ . The other threshold  $s'$  on term ID at each point differs from others in general.

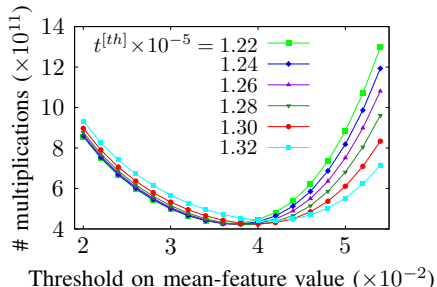


Fig. 14: Actual number of the multiplications along threshold on the mean-feature value with various  $t^{[th]}$  for 8.2M-sized PubMed with  $K=80\,000$ .

multiplications in both the estimated and the actual ones was observed at the identical value of 0.038. Figure 14 shows the actual number of the multiplications when  $t^{[th]}$  was set at the various fixed values from  $1.22 \times 10^5$  to  $1.32 \times 10^5$ . Comparing the approximate number of the multiplications in Fig. 13 with the actual ones in Fig. 14, we notice that the approximate number corresponds to the lowest envelop curve of the actual numbers. Thus, our parameter-estimation algorithm *EstParams* can find appropriate values for  $t^{[th]}$  and  $v^{[th]}$  simultaneously.

#### APPENDIX D ABLATION STUDY

We analyze the contributions of components in our proposed algorithm ES-ICP to its performance. We focus on the main filter ES since the performance of only the auxiliary filter ICP is evaluated in Section VI-D. The ES filter exploits the tight upper bounds on the similarities obtained by using the three regions divided by the two parameters of  $t^{[th]}$  and  $v^{[th]}$ . Depending on whether or not the two parameters are used, we prepared three algorithms without ICP in addition to the baseline MIVI.

The first algorithm was ES that employed both the two parameters. The second was ThV that utilized only the parameter of  $v^{[th]}$  that is estimated by  $t^{[th]} = 0$ <sup>12</sup>. ThV calculated the upper-bound similarities based on the  $v^{[th]}$  in the range of all the term IDs. The upper bounds were looser than those of ES since the exact partial similarities in

<sup>12</sup>ThV's  $v^{[th]}$  was 0.032 while ES's 0.038 for 8.2M-sized PubMed with  $K=80\,000$ .

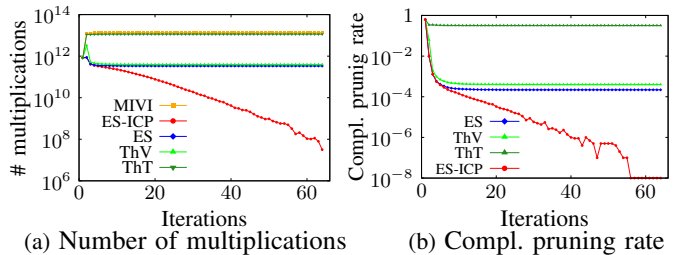


Fig. 15: Ablation study in 8.2M-sized PubMed data set with  $K=80\,000$ : (a) Number of multiplications and (b) Complementary pruning rate along iterations until convergence.

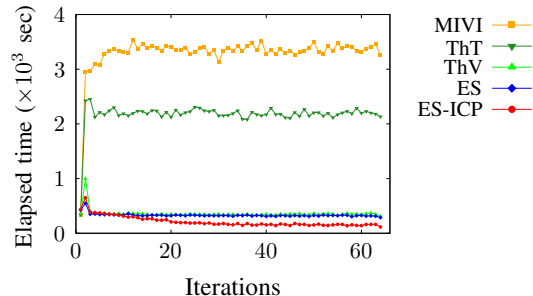


Fig. 16: Elapsed time along iterations until convergence in 8.2M-sized PubMed data set with  $K=80\,000$ .

Region 1 of ES were replaced with the corresponding upper bounds. For calculating the exact similarities of unpruned centroids, ThV needed mean-inverted index  $\check{M}^{p[r]}$  of the memory size of  $\{D \times K \times \text{sizeof}(\text{double})\}$  bytes. Note that ThV's memory size differs from that of ES-ICP, which is  $\{(D - t^{[th]} + 1) \times K \times \text{sizeof}(\text{double})\}$  bytes. The last was ThT that utilized the parameter of  $t^{[th]}$  that is estimated by  $v^{[th]} = 1.0$ <sup>13</sup>. The upper bounds  $\rho_{(j;i)}^{[ub]'}$  corresponding to those in Eq. (4) are expressed by  $\rho_{(j;i)}^{[ub]'} = (\rho 1')_{(j;i)} + \|\mathbf{x}_i^{p'}\|_1$ , where  $\|\mathbf{x}_i^{p'}\|_1$  and  $(\rho 1')_{(j;i)}$  respectively denote the partial  $L_1$  norm of the  $i$ th object and the exact partial similarity of the object to the  $j$ th centroid based on ThT's  $t^{[th]}$ .

Figures 15(a) and (b) respectively show the number of the multiplications (Mult) and the complementary pruning rate (CPR)<sup>14</sup> along iterations until convergence when the algorithms were applied to the 8.2M-sized PubMed with  $K = 80\,000$ . ES and ThV successfully reduced both the multiplications and the CPR at the early stage in the iterations while ThT barely did. This observation shows that ThT had much looser upper bounds than ES and ThV. We know that the ES's pruning performance was mainly supported by the upper bounds based on the parameter  $v^{[th]}$ .

Figure 16 shows the elapsed time that each algorithm required in the same setting in Fig. 15. Table VIII shows the corresponding performance rates of the compared algorithms to ES-ICP. ES and ThV had the similar characteristics to each other in terms of the elapsed time and the performance-

<sup>13</sup>ThT's  $t^{[th]}$  was 140 904 while ES's 128 090 for 8.2M-sized PubMed with  $K=80\,000$ .

<sup>14</sup>The values of CPR were bounded below by  $1 \times 10^{-8}$ .

TABLE VIII  
ABLATION STUDY OF PROPOSED ALGORITHM

Algo.	Avg Mult	Avg time	Inst	BM	LLCM	Max MEM
ES	3.793	1.546	1.782	1.658	3.205	0.998
ThV	4.832	1.676	1.925	1.956	3.461	5.777
ThT	119.4	10.16	13.39	7.173	11.54	0.5094

degradation factors of Inst, BM, and LLCM. ThV needed the high memory capacity for its partial mean-inverted index  $\check{M}^{p[r]}$ . We consider that the difference between these two algorithms and ES-ICP comes from the number of unpruned centroids in Fig. 15. ThT had the inferior performance to the others except the maximum memory usage. This shows that the parameter  $t^{[th]}$  contributed to not the pruning performance but rather the low memory usage for the partial mean-inverted index  $\check{M}^{p[r]}$  of  $\{(D - t^{[th]} + 1) \times K \times \text{sizeof}(\text{double})\}$ -byte capacity. Compared with MIVI in Table IV, ThT slightly decreased Mult and Inst with the aid of its filter while it increased BM and LLCM. This was caused by ThT's poor filter passing many centroids in Fig. 15(b). Then, many branch mispredictions occurred in the conditional branch at the gathering phase, which judges whether or not  $\rho_{(j;i)}^{[ub]}$  is larger than  $\rho_{(max)}$  and mean-feature values in the partial mean-inverted index were loaded many times for the exact similarity calculations.

In reference, the comparisons of actual performance of ES-ICP, ES, ThV, and ThT are shown in Tables IX, X, XI, and XII. Tables IX and X correspond to those when the algorithms were applied to the 8.2M-sized PubMed with  $K = 80\,000$  and Tables XI and XII correspond to those when the algorithms were applied to the 1M-sized NYT data set with  $K = 10\,000$ .

Consequently, the parameters of  $v^{[th]}$  and  $t^{[th]}$  mainly contribute to the high pruning performance and the low memory usage, respectively. The proposed algorithm ES-ICP with the two filters of ES and ICP efficiently worked at high speed and with low memory consumption from the early to the last stage in the iterations.

#### APPENDIX E ALGORITHM PERFORMANCE IN SECTION II

The algorithm performance of MIVI, DIVI and Ding<sup>+</sup> in Section II are shown as the rates to the baseline algorithm MIVI. This section shows the actual values of their performance.

Tables XIII shows the average values per iteration of the number of multiplications and the elapsed time (sec) when the algorithms were executed at an identical initial state in the 8.2M-sized PubMed with  $K = 80\,000$  until the convergence where they needed 64 iterations. Table XIV shows their perf results (total amounts), where the numbers of branches and last-level-cache (LLC) loads are added in addition to the evaluation items in Table II in Section II. We notice two facts in the perf results. One is that Ding<sup>+</sup> and DIVI needed many LLC-loads and respectively caused LLC-load misses of around 99% and 80% of the loads. The other is that Ding<sup>+</sup> failed around 10% of conditional-branch predictions while MIVI did

only 0.04%. These caused the increase of elapsed time of Ding<sup>+</sup> and DIVI.

#### APPENDIX F COMPARED ALGORITHMS IN SECTION VI-D

This section details TA-ICP and CS-ICP in Section VI-D. Both the algorithms employ the mean-inverted index that is partitioned by the structural parameter  $t^{[th]}$  (threshold on term IDs) into two regions like the proposed algorithm ES-ICP. The differences from ES-ICP are in their main upper-bound-based pruning (UBP) filters and data structures related to the filters.

##### A. TA-ICP

TA-ICP is characterized by using (1) the UBP filter every an individual object and (2) two mean-inverted indexes for moving centroids and all the centroids. Each array of the mean-inverted index is sorted in descending order of the mean-feature values. Remind that ES-ICP's array is not sorted but classified in Section IV-A. The UBP filter of TA-ICP is designed, inspired by the threshold algorithm (TA) in Fagin<sup>+</sup> and Li<sup>+</sup> algorithms. This filter utilizes a threshold ( $v_{(ta)i}^{[th]}$ ) on mean-feature values, which is defined every the  $i$ th object by Eq. (16) as follows.

$$v_{(ta)i}^{[th]} = \rho_{(max)} / \|\mathbf{x}_i\|_1,$$

where  $\|\mathbf{x}_i\|_1$  and  $\rho_{(max)}$  denote the  $L_1$ -norm of the  $i$ th object-feature vector and the similarity of  $i$ th object to the centroid to which the object belongs at the last iteration. Due to the threshold for the individual object, it is difficult to structure the mean-inverted index when incorporating the auxiliary ICP filter unlike ES-ICP. TA-ICP employs the two mean-inverted indexes for moving and all the centroids.

Algorithms 8 and 9 show the pseudocodes of the assignment step in TA-ICP. At line 6 in Algorithm 8, the individual threshold is set. In the gathering phase from lines 7 to 11, the candidate-centroid-ID set  $\mathcal{Z}_i$  for exact similarity calculations is made by the UBP and ICP filters. The exact similarity calculations for the centroids with IDs in  $\mathcal{Z}_i$  are performed at lines 12 to 15.  $w'_{(s,j)}$  at line 14 denotes the mean-feature value of the  $j$ th centroid in the  $s$ th array in the partial mean-inverted index that is different from the ES-ICP's counter part in including all the mean-feature values.

Algorithm 9 shows the pseudocode of the candidate-gathering function  $G_{(ta)0}$  at line 11 in Algorithm 8.  $G_{(ta)0}$  is used for the object that does not satisfy the condition in Eq. (5). When calculating the exact partial similarity of the  $i$ th object to the centroids whose ID is  $c_{(s,q)}$ ,  $G_{(ta)0}$  judges whether its feature value satisfies the condition of  $v_{c_{(s,q)}} \geq v_{(ta)i}^{[th]}$  or not at line 6. After the exact partial-similarity calculations in Regions 1 and 2 (defined by  $v_{(ta)i}^{[th]}$ ), the upper bound on the similarity to the centroid whose exact partial-similarity is not zero is calculated. If the exact partial-similarity is zero, the upper bound is smaller than or equal to  $\rho_{(max)}$  from the definition of  $v_{(ta)i}^{[th]} = \rho_{(max)} / \|\mathbf{x}_i\|_1$ . In the gathering phase, the centroid-IDs of the centroids passing through the TA filter are collected in  $\mathcal{Z}_i$ .

**Algorithm 8** Assignment step in TA-ICP

---

```

1: Input:  $\hat{\mathcal{X}}, \check{\mathcal{M}}^{[r-1]}, \check{\mathcal{M}}^{p[r-1]}, \{\rho_{a(i)}^{[r-1]}\}_{i=1}^N, t^{[th]},$ 
 $\check{\mathcal{M}}_{mv}^{[r-1]}$ 
2: Output:  $\mathcal{C}^{[r]} = \{C_j^{[r]}\}_{j=1}^K$ 
3:  $C_j^{[r]} \leftarrow \emptyset, j = 1, 2, \dots, K$ 
    $\triangleright$  Calculate similarities in parallel wrt  $\hat{\mathcal{X}}$ 
4: for all  $\hat{\mathbf{x}}_i = [(t_{(i,p)}, u_{t_{(i,p)}})]_{p=1}^{(nt)_i} \in \hat{\mathcal{X}}$  do
5:    $\mathcal{Z}_i \leftarrow \emptyset, \{\rho_j\}_{j=1}^K \leftarrow 0, \rho_{(max)} \leftarrow \rho_{a(i)}^{[r-1]},$ 
 $\{y_{(i,j)}\}_{j=1}^K \leftarrow \sum_{t_{(i,p)} \geq t^{[th]}} u_{t_{(i,p)}}$ 
6:    $v_{(ta)_i}^{[th]} \leftarrow \rho_{(max)} / \|\mathbf{x}_i\|_1$   $\triangleright$  Individual threshold
    $\triangleright$  Gathering phase
7:   if  $xState = 1$  then  $\triangleright$  Object satisfies Eq. (5).
8:      $\text{args} \leftarrow \mathcal{Z}_i, \{\rho_j, y_{(i,j)}\}_{j=1}^K, \rho_{(max)}, v_{(ta)_i}^{[th]}$ 
9:      $(\mathcal{Z}_i, \{\rho_j\}_{j=1}^K) = G_{(ta)1}(\text{args})$ 
10:   else
11:      $(\mathcal{Z}_i, \{\rho_j\}_{j=1}^K) = G_{(ta)0}(\text{args})$ 
    $\triangleright$  Exact-similarity calculation for unpruned centroids
12:   for  $(s \leftarrow t_{(i,p)}) \geq t^{[th]}$  do
13:     for all  $j \in \mathcal{Z}_i$  do
14:       if  $w'_{(s,j)} < v_{(ta)_i}^{[th]}$  then
15:          $\rho_j \leftarrow \rho_j + u_s \cdot w'_{(s,j)}$ 
    $\triangleright$  Verification phase: The same as that in Algorithm 4.
16:    $C_{a(i)}^{[r]} \leftarrow C_{a(i)}^{[r]} \cup \{\hat{\mathbf{x}}_i\}$ 

```

---

**Algorithm 9** Candidate-gathering function:  $G_{(ta)0}$ 


---

```

Input:  $\hat{\mathbf{x}}_i, \check{\mathcal{M}}^{[r-1]}, t^{[th]},$ 
 $\mathcal{Z}_i, \{\rho_j, y_{(i,j)}\}_{j=1}^K, \rho_{(max)}, v_{(ta)_i}^{[th]}$ 
Output:  $\mathcal{Z}_i, \{\rho_j\}_{j=1}^K$ 
 $\triangleright$  Exact partial similarity calculation
1: for  $(s \leftarrow t_{(i,p)}) < t^{[th]}$  for  $p$  in  $\hat{\mathbf{x}}_i$  do  $\triangleright$  Region 1
2:   for  $1 \leq q \leq (mf)_s$  do
3:      $\rho_{c(s,q)} \leftarrow \rho_{c(s,q)} + u_s \cdot v_{c(s,q)}$ 
4: for  $(s \leftarrow t_{(i,p)}) \geq t^{[th]}$  for  $p$  in  $\hat{\mathbf{x}}_i$  do  $\triangleright$  Region 2
5:   for  $1 \leq q \leq (mf)_s$  do
6:     if  $v_{c(s,q)} < v_{(ta)_i}^{[th]}$  then break
7:      $\rho_{c(s,q)} \leftarrow \rho_{c(s,q)} + u_s \cdot v_{c(s,q)}$ 
8:      $y_{(i,c(s,q))} \leftarrow y_{(i,c(s,q))} - u_s$ 
    $\triangleright$  Gathering phase
9: for  $1 \leq j \leq K$  do
10:   if  $\rho_j = 0$  then continue
11:    $\rho_j^{[ub]} \leftarrow \rho_j + v_{(ta)_i}^{[th]} \cdot y_{(i,j)}$   $\triangleright$  UB calculation
12:   if  $\rho_j^{[ub]} > \rho_{(max)}$  then  $\triangleright$  UBP filter
13:    $\mathcal{Z}_i \leftarrow \mathcal{Z}_i \cup \{j\}$ 

```

---

The function  $G_{(ta)1}$  at line 9 in Algorithm 8 has the identical structure to  $G_{(ta)0}$ . The difference is that  $G_{(ta)1}$  uses the moving-centroid mean-inverted index instead of  $\check{\mathcal{M}}^{[r-1]}$ . For this difference,  $(mf)_s$  at lines 2 and 5 in  $G_{(ta)0}$  is replaced with  $(mfM)_s$  in  $G_{(ta)1}$ .

**B. CS-ICP**

CS-ICP is characterized by using (1) the Cauchy-Schwarz inequality that is applied to mean-feature vectors in a subspace

**Algorithm 10** Assignment step in CS-ICP

---

```

Input:  $\hat{\mathcal{X}}, \check{\mathcal{M}}^{[r-1]}, \check{\mathcal{M}}^{p[r-1]}, \{\rho_{a(i)}^{[r-1]}\}_{i=1}^N, \{\|\mathbf{x}_i^p\|_2\}_{i=1}^N,$ 
 $\check{\mathcal{M}}_{sq}^{p[r-1]}, t^{[th]}$ 
Output:  $\mathcal{C}^{[r]} = \{C_j^{[r]}\}_{j=1}^K$ 
1:  $C_j^{[r]} \leftarrow \emptyset, j = 1, 2, \dots, K$ 
    $\triangleright$  Calculate similarities in parallel wrt  $\hat{\mathcal{X}}$ 
2: for all  $\hat{\mathbf{x}}_i = [(t_{(i,p)}, u_{t_{(i,p)}})]_{p=1}^{(nt)_i} \in \hat{\mathcal{X}}$  do
3:    $\{\rho_j\}_{j=1}^K \leftarrow 0, \mathcal{Z}_i \leftarrow \emptyset, \rho_{(max)} \leftarrow \rho_{a(i)}^{[r-1]}$ 
    $\triangleright$  Gathering phase
4:   if  $xState = 1$  then  $\triangleright$  Object satisfies Eq. (5).
5:      $(\mathcal{Z}_i, \{\rho_j\}_{j=1}^K) = G_{(cs)1}(\mathcal{Z}_i, \{\rho_j\}_{j=1}^K, \rho_{(max)})$ 
6:   else
7:      $(\mathcal{Z}_i, \{\rho_j\}_{j=1}^K) = G_{(cs)0}(\mathcal{Z}_i, \{\rho_j\}_{j=1}^K, \rho_{(max)})$ 
    $\triangleright$  Exact-similarity calculation for unpruned centroids:
   The same algorithm structure as that in Algorithm 4
    $\triangleright$  Verification phase: The same as that in Algorithm 4
8:    $C_{a(i)}^{[r]} \leftarrow C_{a(i)}^{[r]} \cup \{\hat{\mathbf{x}}_i\}$ 

```

---

**Algorithm 11** Candidate-gathering function:  $G_{(cs)0}$ 


---

```

Input:  $\hat{\mathbf{x}}_i, \check{\mathcal{M}}^{[r-1]}, \mathcal{Z}_i, \{\rho_j\}_{j=1}^K, \rho_{(max)}, t^{[th]},$ 
 $\|\mathbf{x}_i^p\|_2, \check{\mathcal{M}}_{sq}^{p[r-1]}$ 
Output:  $\mathcal{Z}_i, \{\rho_j\}_{j=1}^K$ 
1:  $\{\|\mu_j^p\|_2^2\}_{j=1}^K \leftarrow 0$   $\triangleright$  Initialization
    $\triangleright$  Exact partial similarity calculation
2: for  $(s \leftarrow t_{(i,p)}) < t^{[th]}$  in all term IDs in  $\hat{\mathbf{x}}_i$  do
3:   for  $1 \leq q \leq (mf)_s$  do
4:      $\rho_{c(s,q)} \leftarrow \rho_{c(s,q)} + u_s \cdot v_{c(s,q)}$ 
    $\triangleright$  Calculate squared mean-L2-norm in object-subspace
5: for  $(s \leftarrow t_{(i,p)}) \geq t^{[th]}$  in all term IDs in  $\hat{\mathbf{x}}_i$  do
6:   for  $1 \leq q \leq (mf)_s$  do
7:      $\|\mu_{c(s,q)}^p\|_2^2 \leftarrow \|\mu_{c(s,q)}^p\|_2^2 + v_{c(s,q)}^2$ 
    $\triangleright$  Gathering phase
8: for  $1 \leq j' \leq (nMv)$  do  $\triangleright$  nMv: #moving centroids
9:    $j'$  is transformed to  $j$ .
10:    $\rho_j^{[ub]} \leftarrow \rho_j + \|\mathbf{x}_i^p\|_2 \times \sqrt{\|\mu_j^p\|_2^2}$   $\triangleright$  UB calculation
11:   if  $\rho_j^{[ub]} > \rho_{(max)}$  then  $\triangleright$  UBP filter
12:    $\mathcal{Z}_i \leftarrow \mathcal{Z}_i \cup \{j\}$ 

```

---

of an individual object-feature vector, (2) an additional mean-inverted index that stores squared mean-feature values, and (3) no threshold on the mean-feature values unlike ES-ICP and TA-ICP.

Algorithm 10 shows the pseudocode of the assignment step in CS-ICP. The  $\|\mathbf{x}_i^p\|_2$  and  $\check{\mathcal{M}}_{sq}^{p[r-1]}$  in the inputs respectively denote the  $L_2$ -norm of the  $i$ th object's *partial* feature vector and the *partial* squared mean-inverted index in the range of the term IDs ( $s$ ) satisfying  $s \geq t^{[th]}$ . At lines 5 to 7, the candidate centroids for the exact similarity calculations are collected by the candidate-gathering functions  $G_{(cs)0}$  and  $G_{(cs)1}$ . The other parts have the same algorithm structure as those in Algorithm 4 although each array in the partial mean-feature-inverted index for CS-ICP contains all the mean-feature values unlike ES-ICP whose array contains mean-feature values smaller than  $v^{[th]}$  in Region 3.

Algorithm 11 shows the pseudocode of the candidate-

gathering function  $G_{(cs)0}$  at line 7 in Algorithm 10.  $G_{(cs)0}$  is used for the object that does not satisfy the condition in Eq. (5). At lines 2 to 4, the exact partial similarities  $\rho_{c(s,q)}$  are calculated in the range of  $t_{(i,p)} < t^{[th]}$ . At lines 5 to 7, the squared  $L_2$ -norm of the partial mean-feature vector  $\|\mu_{c(s,q)}^p\|_2^2$  is calculated in the subspace of the  $i$ th object-feature vector, where  $v_{c(s,q)}^2$  denotes the squared mean-feature value in  $\mathcal{M}_{sq}^{p[r-1]}$ . At lines 8 to 12, the gathering phase is performed and the centroid-ID set  $\mathcal{Z}_i$  for exact similarity calculations is returned. At line 10, the upper bound on the similarity to the  $j$ th centroid  $\rho_j^{[ub]}$  is calculated by the sum of the foregoing exact partial similarity  $\rho_j$  and the product of the pre-calculated  $L_2$ -norm of the  $i$ th object’s partial feature vector  $\|\mathbf{x}_i^p\|_2$  and  $\sqrt{\|\mu_{c(s,q)}^p\|_2^2}$ . In this product calculation, the square-root operation is performed, which requires high computational cost.

The function  $G_{(cs)1}$  at line 5 in Algorithm 10 is similar to  $G_{(cs)0}$ . The difference is in the endpoint of the loops at lines 3 and 6.  $G_{(cs)0}$  uses  $(mf)_s$  while  $G_{(cs)1}$  does  $(mfM)_s$  in the mean-inverted index consisting of the moving centroids.

### C. Performance Comparison

This section shows the actual performance of ES-ICP, ICP, CS-ICP, and TA-ICP when they were applied to the 8.2M-sized PubMed data set with  $K = 80\,000$  in Tables XV and XVI and the 1M-sized NYT data set with  $K = 10\,000$  in Tables XVII and XVIII.

From the both results in the two distinct data sets and settings, in addition to the facts described in Section VI-D, we note the following two facts. (1) CS-ICP and TA-ICP required more elapsed time than the baseline ICP although they operated using the smaller or around equal number of (completed) instructions or multiplications. This is because they caused the larger numbers of branch mispredictions (BMs) and last-level-cache misses (LLCMs). In particular, TA-ICP did much more branch mispredictions than the others while their numbers of branch instructions were not much different. This led to its worse performance. (2) The elapsed-time differences of the four algorithms came from those in the assignment step which we focused on. The four algorithms worked in not much different average update time although they constructed the different data structures. In particular, ES-ICP and CS-ICP took less update time than the baseline ICP because they processed fewer centroids owing to their high pruning rates.

In the NYT results in Table XVII, we note that surprisingly, ES-ICP took less elapsed time in the assignment step than that in the update step. For any further acceleration in such data sets and settings, we will need to change our strategy of the acceleration in the assignment step to that in both the steps including the update.

These, in addition to the results in Section VI-D, show that only reducing the numbers of multiplications or instructions does not always lead to reducing elapsed time required by an algorithm. Suppressing the performance-degradation factors in Section II realizes the acceleration. In other words, by carefully designing an algorithm so that it suppresses the

numbers of instructions, last-level cache misses (LLCMs), and branch mispredictions (BMs), we can obtain an efficient algorithm that operates in the *architecture-friendly manner*.

We also note that reducing the maximum memory size required by ES-ICP, which is described as the remaining task in Section VI-D, is not a serious problem with respect to the actual memory size and the LLCMs in the current data sets and settings from Tables XV and XVII. The memory sizes used for the partial mean-inverted indexes  $\mathcal{M}^{p[r]}$  in the 8.2M-sized PubMed and 1M-sized NYT data sets in the foregoing settings were around 8.3 GB and 3.2 GB, respectively. Even for the PubMed data set, total amount size was 16.72 GB. A current standard computer system for scientific and technical computing equips a memory system whose size is much larger than the foregoing amount. Regarding LLCMs, the number of accesses to  $\mathcal{M}^{p[r]}$  were small, i.e.,  $\mathcal{M}^{p[r]}$  was rarely loaded to the caches because ES-ICP’s filters reduced unpruned centroids that were targets for exact similarity calculations using  $\mathcal{M}^{p[r]}$ .

## APPENDIX G MAIN-FILTER COMPARISON

There may be a doubt of the combination of the main UBP and auxiliary ICP filters in the compared algorithms weakens the main filter’s positive effect on the performance. To clear up the doubt, this section compares only the main filters of ES-ICP, TA-ICP, and CS-ICP, where algorithms with the filters are respectively called ES-MIVI, TA-MIVI, and CS-MIVI. The algorithms were applied to the 8.2M-sized PubMed data set with  $K = 80\,000$  in Tables XIX and XX and the 1M-sized NYT data set with  $K = 10\,000$  in Tables XXI and XXII.

The most important fact is that no algorithm without the ICP filter improved its elapsed time in the data sets and settings, compared with the corresponding algorithm with the ICP filter. This is because the algorithm with the ICP filter suppressed the performance-degradation factors of the numbers of instructions, branch mispredictions (BMs), and last-level-cache misses (LLCMs).

ES-MIVI showed the best performance regardless of the data sets and settings. We note that the ES filter was effective by itself and from the ES-ICP’s results in Tables XV to XVIII, both the filters of ES and ICP worked without losing each other’s advantages. When combining plural filters like the UBP and ICP filters, we should carefully design the combined algorithm that operates in the *architecture-friendly manner*.

## APPENDIX H INITIAL-STATE INDEPENDENCE

We deal with a large-scale and high-dimensional sparse document data set and partition it into numerous classes, i.e., use a huge  $K$  value (Section I). Compared with widely-used Lloyd-type  $K$ -means settings in the metric space, this setting differs in data size  $N$ , dimensionality  $D$ , and number of clusters  $K$ . It is often said that  $K$ -means clustering performance strongly depends on an initial state, i.e., seeding [55]. In our setting, however, algorithm performance is independent of initial states.

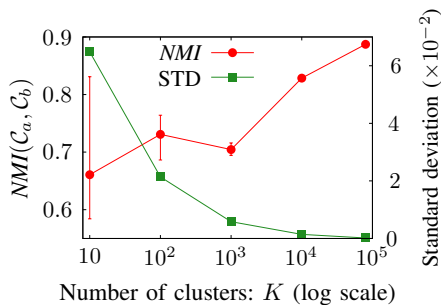


Fig. 17: *NMI* of clustering results for 8.2M-sized PubMed.

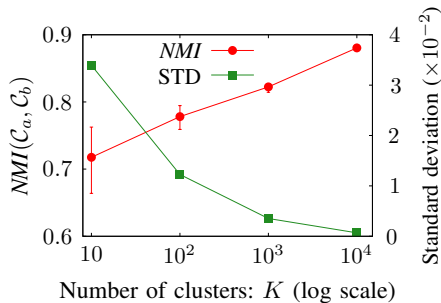


Fig. 18: *NMI* of clustering results for 1M-sized NYT.

In a high-dimensional metric space, object vectors are located far away from each other and an average and a variance of their distances are very large and small, respectively [56], [57]. Such a phenomenon has been called the curse of dimensionality [58]. Similarly, the phenomenon occurs in a high-dimensional hypersphere in the spherical  $K$ -means setting. In this setting, we consider that a seeding method randomly choosing an initial state yields a similar result to a commonly used one in  $K$ -means++ [59].

We observed in our preliminary experiments that when an algorithm started at different initial states, the resultant values of two distinct evaluation measures [60] did not change so much. One of the two measures is an objective function value at convergence, which is represented by

$$J(\mathcal{C}_h) = \sum_{C_j \in \mathcal{C}_h} \sum_{\mathbf{x}_i \in C_j} \mathbf{x}_i \cdot \boldsymbol{\mu}_j \quad (47)$$

$$J = \left(\frac{1}{L}\right) \sum_{1 \leq h \leq L} J(\mathcal{C}_h), \quad (48)$$

where  $\mathcal{C}_h$  denotes the clustering result obtained by the  $h$ th initial states ( $h = 1, 2, \dots, L$ ) and  $L$  is the number of the prepared initial states. The other is normalized mutual information *NMI*. Given two clustering results  $\mathcal{C}_a$  and  $\mathcal{C}_b$ ,  $NMI(\mathcal{C}_a, \mathcal{C}_b)$  is defined by

$$NMI(\mathcal{C}_a, \mathcal{C}_b) = \frac{\mathcal{I}(\mathcal{C}_a, \mathcal{C}_b)}{\sqrt{\mathcal{H}(\mathcal{C}_a)\mathcal{H}(\mathcal{C}_b)}}, \quad (49)$$

where  $\mathcal{I}(\mathcal{C}_a, \mathcal{C}_b)$  and  $\mathcal{H}(\mathcal{C}_a)$  denote the mutual information between  $\mathcal{C}_a$  and  $\mathcal{C}_b$  and the entropy of  $\mathcal{C}_a$ , respectively [61]. When the  $L$  initial states are given to an algorithm, *NMI* is expressed by

$$NMI = \left(1/\binom{L}{2}\right) \sum_{\substack{1 \leq a, b \leq L \\ a \neq b}} NMI(\mathcal{C}_a, \mathcal{C}_b). \quad (50)$$

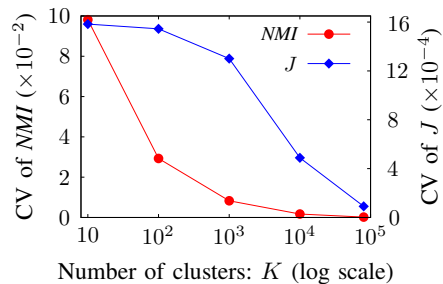


Fig. 19: Coefficient of variations (CV) of objective function value  $J$  and *NMI* of clustering results for 8.2M-sized PubMed.

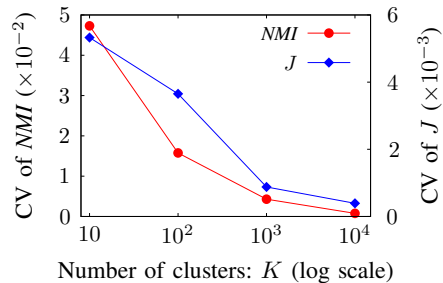


Fig. 20: Coefficient of variations (CV) of objective function value  $J$  and *NMI* of clustering results for 1M-sized NYT.

A larger value of  $J(\mathcal{C}_h)$  means that  $\mathcal{C}_h$  is a better clustering result and if  $J(\mathcal{C}_a) \sim J(\mathcal{C}_b)$ ,  $\mathcal{C}_a$  is almost equivalent to  $\mathcal{C}_b$  in terms of optimization.  $NMI(\mathcal{C}_a, \mathcal{C}_b)$  measures the similarity between the two clustering results of  $\mathcal{C}_a$  and  $\mathcal{C}_b$ . A larger value of  $NMI(\mathcal{C}_a, \mathcal{C}_b)$  means that the two clustering results are more similar. If  $NMI(\mathcal{C}_a, \mathcal{C}_b) = 1$ ,  $\mathcal{C}_a$  and  $\mathcal{C}_b$  are completely identical.

To confirm experimentally that the sensitivity of an initial state is very low in our setting, in particular, at large  $K$  values, we evaluated the two measures, varying the  $K$  values of our proposed algorithm in both the 8.2M-sized PubMed and the 1M-sized NYT data set. In the 8.2M-sized PubMed data set, the five  $K$  values of 10, 100, 1000, 10000, and 80000 were used while the four values except 80000 were done in the 1M-sized NYT. The proposed algorithm with each of the foregoing  $K$  values started at the different 10 initial states chosen randomly.

Figures 17 and 18 show the values of  $NMI(\mathcal{C}_a, \mathcal{C}_b)$  and their standard deviations in the 8.2M-sized PubMed and the 1M-sized NYT data set, respectively. Both the results show the similar tendency that the *NMI* values increased and the standard deviations decreased with  $K$ . For the huge  $K$  values, the *NMI* values approached 0.9. Even when  $K = 10$ , the *NMI* values were around 0.7. This shows that the clustering results obtained by randomly chosen different initial states were very similar in our setting.

Furthermore, we utilized as statistics of the two measures a coefficient of variation (CV) that is expressed as

$$CV = \frac{\sigma_z}{\bar{z}}, \quad (51)$$

where  $\sigma_z$  and  $\bar{z}$  denote the standard deviation and the average of variable  $z$ , respectively, and  $z$  means  $J$  or *NMI* in our case. A smaller CV of  $z$  represents that the  $z$ 's variation is smaller. Figures 19 and 20 show the CV's of the objective

function values  $J$  and the normalized mutual information  $NMI$  in the 8.2M-sized PubMed and the 1M-sized NYT data set, respectively. We know that the  $CV$ 's of  $J$  and  $NMI$  decreased with  $K$ . Thus, the clustering results are independent of the initial states in our setting of using the large values of  $N$ ,  $D$ , and  $K$ .

## APPENDIX I PARETO-PRINCIPLE-LIKE PHENOMENON

We observed in our preliminary experiments that a *cumulative partial similarity* of an object to a centroid and a *normalized rank* of each partial similarity have a relationship like the Pareto principle [62]. We first define both the cumulative partial similarity and the normalized rank. Consider that we calculate a similarity  $\rho_{a(i)}$  between the  $i$ th object  $\mathbf{x}_i$  and centroid  $\boldsymbol{\mu}_{a(i)}$  of the cluster which  $\mathbf{x}_i$  belongs to. The similarity  $\rho_{a(i)}$  is expressed by

$$\rho_{a(i)} = \sum_{p=1}^{(nt)_i} u_{t(i,p)} \cdot \mu_{(a(i),t(i,p))}, \quad (52)$$

where  $\mu_{(a(i),t(i,p))}$  denotes the element of  $\boldsymbol{\mu}_{a(i)}$  whose term ID is  $t(i,p)$ ,  $u_{t(i,p)}$  the object-feature value whose term ID is  $t(i,p)$ , and  $(nt)_i$  the number of distinct terms which the object  $\mathbf{x}_i$  uses (Table I). We sort the partial similarities  $[u_{t(i,p)} \cdot \mu_{(a(i),t(i,p))}]_{p=1}^{(nt)_i}$  in descending order and express the  $h$ th rank's partial similarity as  $\delta\rho_{a(i)}(h)$ ,  $h = 1, 2, \dots, (nt)_i$ . Note that  $h$  corresponds to the number of multiplications for the partial similarity calculation. Then, the normalized rank  $NR(i, h)$  and the cumulative partial similarity  $CPS(i, h)$  are respectively expressed by

$$NR(i, h) = \frac{h}{(nt)_i} \quad (53)$$

$$CPS(i, h) = \frac{1}{\rho_{a(i)}} \sum_{h'=1}^h \delta\rho_{a(i)}(h'), \quad (54)$$

where  $CPS(i, (nt)_i) = 1$ . For statistical processing with regard to all the object, we introduce ordered bin instead of  $NR(i, h)$ . We rename the foregoing  $NR(i, h)$  an individual normalized rank and the ordered bin a normalized rank again. The normalized ranks (ordered bins)  $NR(\hat{h})$  are discrete values aligned at regular intervals expressed as  $\delta b$ , where  $\hat{h}$  denotes the bin ID of an integer from 0 to  $1/\delta b$ . For instance, if  $\delta b = 0.01$ , then  $0 \leq (\hat{h} \in \mathbb{Z}) \leq 100$ . An average  $CPS$  with regard to all the objects,  $\overline{CPS}(\hat{h})$ , is defined by

$$NR(\hat{h}) = \hat{h} \cdot \delta b \quad (55)$$

$$\overline{CPS}(\hat{h}) = \frac{1}{N} \sum_{i=1}^N CPS(i, ((nt)_i \cdot NR(\hat{h}))), \quad (56)$$

where if  $(nt)_i \cdot NR(\hat{h}) \notin \{NR(i, h)\}$ ,  $CPS(i, ((nt)_i \cdot NR(\hat{h})))$  is calculated with linear interpolation.

Figures 21 and 22 show  $\overline{CPS}(\hat{h})$  and its standard deviation  $STD(\hat{h})$  against  $NR(\hat{h})$  when a spherical  $K$ -means algorithm was applied to the 8.2M-sized PubMed data set with  $K = 80\,000$  and the 1M-sized NYT with  $K = 10\,000$ , respectively. In each figure, the two curves for each of  $\overline{CPS}$  and  $STD$  are

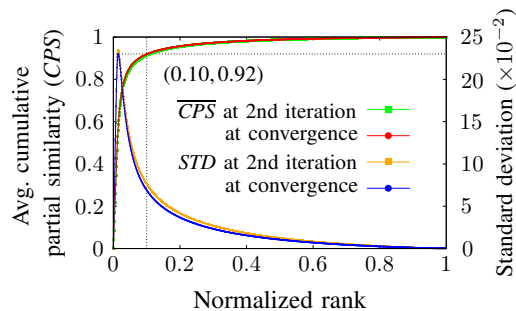


Fig. 21: Average cumulative partial similarity ( $CPS$ ) and its standard deviation ( $STD$ ) against normalized rank when a spherical  $K$ -means algorithm with  $K=80\,000$  was applied to the 8.2M-sized PubMed.

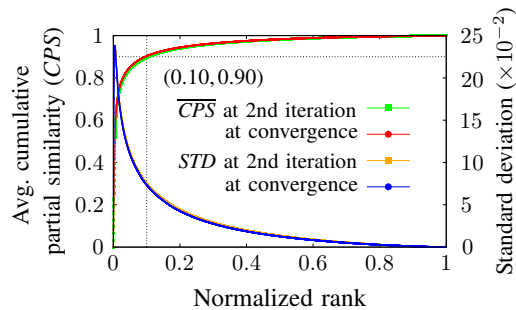


Fig. 22: Average cumulative partial similarity ( $CPS$ ) and its standard deviation ( $STD$ ) against normalized rank when a spherical  $K$ -means algorithm with  $K=10\,000$  was applied to the 1M-sized NYT.

depicted, which correspond to those at the second iteration and at the convergence. The two curves of  $\overline{CPS}$  in both the figures showed the almost similar characteristics that increased rapidly and reached 1.0, despite the number of iterations (at the second or convergence). In particular,  $\overline{CPS}(0.1) = 0.92, 0.90$  in the 8.2M-sized PubMed and the 1M-sized NYT data set, respectively. Besides, the standard deviations at each normalized rank were small. These characteristics seem like Pareto principle, i.e., a large fraction of a similarity is calculated at a very low cost.

## APPENDIX J PRUNING BASED ON TRIANGLE INEQUALITY

We describe a typical triangle-inequality-based pruning method while referring to Fig. 23. Let  $d(\mathbf{x}_i, \boldsymbol{\mu}_j^{[r-1]})$  denote the distance between  $\mathbf{x}_i$  and  $\boldsymbol{\mu}_j^{[r-1]}$  and  $\delta_j^{[r-1]}$  denote the moving distance between  $\boldsymbol{\mu}_j^{[r-1]}$  and  $\boldsymbol{\mu}_j^{[r-2]}$ , where the superscript  $[r-1]$  denotes the  $(r-1)$ th iteration.  $d_{LB}$  is the abbreviation of  $d_{LB}(\mathbf{x}_i, \boldsymbol{\mu}_j^{[r-1]})$  that is the lower bound on  $d(\mathbf{x}_i, \boldsymbol{\mu}_j^{[r-1]})$ . Similarly,  $d_{UB}$  is that of  $d_{UB}(\mathbf{x}_i, \boldsymbol{\mu}_{a(i)}^{[r-1]})$ . Note that when the distance is used as a measure like in this case, we focus on the lower bound on the distance between an object and a mean (centroid) unlike in the case of a similarity measure.

Consider which centroid of  $\boldsymbol{\mu}_{a(i)}^{[r-1]}$  or  $\boldsymbol{\mu}_j^{[r-1]}$  is closer to  $\mathbf{x}_i$ , given the two centroids' distances to  $\mathbf{x}_i$  at the  $(r-2)$ th iteration and the moving distances of the centroids between the  $(r-2)$ th and the  $(r-1)$ th iteration, i.e.,  $\delta_j^{[r-1]}$  and  $\delta_{a(i)}^{[r-1]}$ . We apply the triangle inequality to the three points of  $\mathbf{x}_i$ ,  $\boldsymbol{\mu}_{(*)}^{[r-2]}$ , and  $\boldsymbol{\mu}_{(*)}^{[r-1]}$  under the condition of  $\delta_{(*)}^{[r-1]}$  and  $d_{(*)}(\mathbf{x}_i, \boldsymbol{\mu}_{(*)}^{[r-2]})$



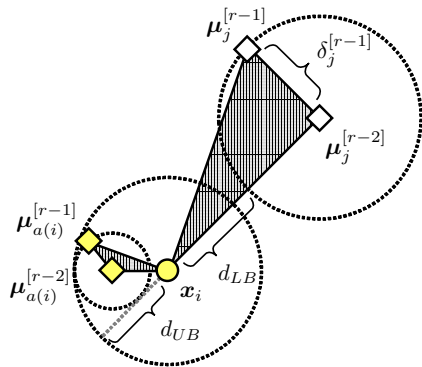


Fig. 23: Typical usage of the triangle inequality for omitting the exact distance calculation of object  $x_i$  to centroid  $\mu_j$  in a metric space. The distance calculation is omitted if  $d_{UB} \leq d_{LB}$ .

are known, where the subscript  $(*)$  denotes either  $j$  or  $a(i)$ . Then  $d_{LB}$  and  $d_{UB}$  are expressed by

$$d_{LB}(x_i, \mu_j^{[r-1]}) = |d(x_i, \mu_j^{[r-2]}) - \delta_j^{[r-1]}| \quad (57)$$

$$d_{UB}(x_i, \mu_{a(i)}^{[r-1]}) = d(x_i, \mu_{a(i)}^{[r-2]}) + \delta_{a(i)}^{[r-1]}. \quad (58)$$

If  $d_{UB} < d_{LB}$ , then we know that  $\mu_{a(i)}^{[r-1]}$  is closer to  $x_i$ . As a result, we can omit calculations of the exact distance of  $x_i$  to  $\mu_{(*)}^{[r-1]}$ . In the pruning method, a key distance is the moving distance such as  $\delta_{(*)}^{[r-1]}$ . Note that we can use the exact distance of  $d(x_i, \mu_{a(i)}^{[r-1]})$  instead of  $d_{UB}$ . The lower bound tightens as the moving distance becomes smaller. Then more centroids are pruned, causing acceleration. This acceleration becomes effective only around the last stage before the convergence where most of the centroids are invariant or slightly move. In our setting, it is not efficient as stated in Section II. It is desired that the acceleration goes through all the iterations, particularly from the early to the middle stage.

## REFERENCES

- [55] M. E. Celebi, H. A. Kingravi, and P. A. Vela, "A comparative study of efficient initialization methods for the k-means clustering algorithm," *Expert Systems with Applications*, vol. 40, no. 1, pp. 200–210, 2013.
- [56] E. Chávez, G. Navarro, R. Baeza-Yates, and J. L. Marroquín, "Searching in metric spaces," *ACM Computing Surveys*, vol. 33, no. 3, pp. 273–321, 2001.
- [57] K. S. Beyer, J. Goldstein, R. Ramakrishnan, and U. Shaft, "When is "Nearest Neighbor" meaningful?" in *Proc. 7th Int. Conf. on Database Theory*, 1999, pp. 217–235.
- [58] R. Bellman, "Dynamic programming," *Science*, vol. 153, no. 3731, pp. 34–37, 1966.
- [59] D. Arthur and S. Vassilvitskii, "k-means++: The advantages of careful seeding," in *Proc. 18th annu. ACM-SIAM Symp. Discrete Algorithms (SODA)*, January 2007, pp. 1027–1035.
- [60] S. Wagner and D. Wagner. (2007) Comparing clusterings - an overview. Karlsruhe Institute of Technology (KIT). [Online]. Available: <https://publikationen.bibliothek.kit.edu/1000011477>
- [61] A. Strehl and J. Ghosh, "Cluster ensembles - a knowledge reuse framework for combining multiple partitions," *Journal of Machine Learning Research*, vol. 3, pp. 583–617, 2002.
- [62] M. E. J. Newman, "Power laws, Pareto distributions and Zipf's law," *Contemporary Physics*, vol. 46, no. issue 5, pp. 323–351, 2005. [Online]. Available: <https://doi.org/10.1080/00107510500052444>

TABLE IX

ABLATION STUDY IN TERMS OF AVERAGE NUMBER OF MULTIPLICATIONS AND AVERAGE ELAPSED TIME UNTIL CONVERGENCE IN 8.2M-SIZED PUBMED WITH K=80 000. NUMBER OF ITERATIONS UNTIL CONVERGENCE IS 64.

Algorithm	Avg. # multiplications per iteration	Avg. elapsed time per iteration (sec): [assignment, update] <sup>†</sup>	Maximum memory size (GB)
ES-ICP	$9.391 \times 10^{10}$	213.8 [185.5, 28.79]	16.72
ES	$3.562 \times 10^{11}$	330.6 [304.0, 27.00]	16.69
ThV	$4.538 \times 10^{11}$	358.4 [329.37, 29.50]	96.59
ThT	$1.122 \times 10^{13}$	2172 [2149, 23.81]	8.52

<sup>†</sup> The average elapsed time does not exactly match the sum of the assignment and the update time because the algorithm terminated at the end of the assignment step of the last iteration.

TABLE X

ABLATION STUDY IN TERMS OF PERF RESULTS UNTIL CONVERGENCE IN 8.2M-SIZED PUBMED WITH K=80 000. NUMBER OF ITERATIONS UNTIL CONVERGENCE IS 64.

Algorithm	# instructions	# branches	# branch misses (%)	# LLC-loads	# LLC-loads misses (%)
ES-ICP	$6.157 \times 10^{14}$	$8.417 \times 10^{13}$	$9.569 \times 10^{10}$ (0.11)	$1.043 \times 10^{13}$	$1.738 \times 10^{12}$ (16.7)
ES	$1.097 \times 10^{15}$	$1.659 \times 10^{14}$	$1.586 \times 10^{11}$ (0.10)	$3.586 \times 10^{13}$	$5.569 \times 10^{12}$ (15.53)
ThV	$1.185 \times 10^{15}$	$1.725 \times 10^{14}$	$1.872 \times 10^{11}$ (0.11)	$4.218 \times 10^{13}$	$6.015 \times 10^{12}$ (14.26)
ThT	$8.244 \times 10^{15}$	$9.009 \times 10^{14}$	$6.864 \times 10^{12}$ (0.08)	$2.713 \times 10^{14}$	$2.004 \times 10^{13}$ (7.39)

TABLE XI

ABLATION STUDY IN TERMS OF AVERAGE NUMBER OF MULTIPLICATIONS AND AVERAGE ELAPSED TIME UNTIL CONVERGENCE IN 1M-SIZED NYT WITH K=10 000. NUMBER OF ITERATIONS UNTIL CONVERGENCE IS 81.

Algorithm	Avg. # multiplications per iteration	Avg. elapsed time per iteration (sec): [assignment, update] <sup>†</sup>	Maximum memory size (GB)
ES-ICP	$2.411 \times 10^{10}$	15.77 [5.394, 10.50]	7.914
ES	$9.411 \times 10^{10}$	26.00 [15.72, 10.41]	7.907
ThV	$1.430 \times 10^{11}$	32.79 [21.99, 10.94]	43.00
ThT	$2.385 \times 10^{12}$	238.5 [229.6, 9.016]	4.752

<sup>†</sup> The average elapsed time does not exactly match the sum of the assignment and the update time because the algorithm terminated at the end of the assignment step of the last iteration.

TABLE XII

ABLATION STUDY IN TERMS OF PERF RESULTS UNTIL CONVERGENCE IN 1M-SIZED NYT DATA SET WITH K=10 000. NUMBER OF ITERATIONS UNTIL CONVERGENCE IS 81.

Algorithm	# instructions	# branches	# branch misses (%)	# LLC-loads	# LLC-loads misses (%)
ES-ICP	$7.003 \times 10^{13}$	$1.239 \times 10^{13}$	$4.127 \times 10^{10}$ (0.33)	$8.470 \times 10^{11}$	$1.044 \times 10^{11}$ (12.3)
ES	$1.538 \times 10^{14}$	$1.993 \times 10^{13}$	$7.044 \times 10^{10}$ (0.35)	$3.046 \times 10^{12}$	$2.727 \times 10^{11}$ (8.95)
ThV	$1.931 \times 10^{14}$	$2.324 \times 10^{13}$	$7.395 \times 10^{10}$ (0.32)	$3.408 \times 10^{12}$	$4.071 \times 10^{11}$ (11.95)
ThT	$2.017 \times 10^{15}$	$2.091 \times 10^{14}$	$8.155 \times 10^{10}$ (0.04)	$2.508 \times 10^{13}$	$2.215 \times 10^{12}$ (8.83)

TABLE XIII

PERFORMANCE OF MIVI, DIVI, AND DING<sup>+</sup> IN 8.2M-SIZED PUBMED DATA SET WITH K=80 000. NUMBER OF ITERATIONS UNTIL CONVERGENCE IS 64.

Algorithm	Avg. # multiplications per iteration	Avg. elapsed time per iteration (sec)
MIVI	$1.326 \times 10^{13}$	$3.302 \times 10^3$
DIVI	$1.326 \times 10^{13}$	$3.372 \times 10^4$
Ding <sup>+</sup>	$3.029 \times 10^{12}$	$9.552 \times 10^3$

TABLE XIV  
PERF RESULTS OF MIVI, DIVI, AND DING<sup>+</sup> IN 8.2M-SIZED PUBMED DATA SET WITH K=80000.  
NUMBER OF ITERATIONS UNTIL CONVERGENCE IS 64.

Algorithm	# instructions	# branches	# branch misses (%)	# LLC-loads	# LLC-loads misses (%)
MIVI	$1.024 \times 10^{16}$	$1.013 \times 10^{15}$	$3.929 \times 10^{11}$ (0.04)	$2.790 \times 10^{14}$	$1.767 \times 10^{13}$ (6.33)
DIVI	$1.006 \times 10^{16}$	$1.019 \times 10^{15}$	$2.743 \times 10^{12}$ (0.27)	$7.983 \times 10^{14}$	$6.444 \times 10^{14}$ (80.7)
Ding <sup>+</sup>	$6.691 \times 10^{15}$	$1.949 \times 10^{15}$	$1.937 \times 10^{14}$ (9.94)	$6.637 \times 10^{14}$	$6.577 \times 10^{14}$ (99.1)

TABLE XV  
PERFORMANCE COMPARISON OF ES-ICP, ICP, CS-ICP AND TA-ICP IN 8.2M-SIZED PUBMED DATA SET WITH K=80000.  
NUMBER OF ITERATIONS UNTIL CONVERGENCE IS 64.

Algorithm	Avg. # multiplications per iteration	Avg. elapsed time per iteration (sec): [assignment, update] <sup>†</sup>	Maximum memory size (GB)
ES-ICP	$9.391 \times 10^{10}$	204.8 [176.4, 28.86]	16.72
ICP	$2.960 \times 10^{12}$	759.5 [729.9, 30.05]	8.285
CS-ICP	$1.733 \times 10^{11}$	901.7 [875.2, 26.99]	18.31
TA-ICP	$9.069 \times 10^{11}$	1042 [1006, 36.35]	19.07

<sup>†</sup> The average elapsed time does not exactly match the sum of the assignment and the update time because the algorithm terminated at the end of the assignment step of the last iteration.

TABLE XVI  
PERF RESULTS OF ES-ICP, ICP, CS-ICP, AND TA-ICP IN 8.2M-SIZED PUBMED DATA SET WITH K=80000.  
NUMBER OF ITERATIONS UNTIL CONVERGENCE IS 64.

Algorithm	# instructions	# branches	# branch misses (%)	# LLC-loads	# LLC-loads misses (%)
ES-ICP	$6.197 \times 10^{14}$	$8.471 \times 10^{13}$	$9.623 \times 10^{10}$ (0.11)	$1.037 \times 10^{13}$	$1.619 \times 10^{12}$ (15.6)
ICP	$2.876 \times 10^{15}$	$2.934 \times 10^{14}$	$2.796 \times 10^{11}$ (0.10)	$8.277 \times 10^{13}$	$4.467 \times 10^{12}$ (5.40)
CS-ICP	$2.346 \times 10^{15}$	$2.786 \times 10^{14}$	$3.127 \times 10^{11}$ (0.11)	$9.297 \times 10^{13}$	$8.025 \times 10^{12}$ (8.63)
TA-ICP	$1.476 \times 10^{15}$	$2.067 \times 10^{14}$	$1.859 \times 10^{12}$ (0.90)	$4.593 \times 10^{13}$	$2.209 \times 10^{13}$ (48.10)

TABLE XVII  
PERFORMANCE COMPARISON OF ES-ICP, ICP, CS-ICP AND TA-ICP IN 1M-SIZED NYT DATA SET WITH K=10000.  
NUMBER OF ITERATIONS UNTIL CONVERGENCE IS 81.

Algorithm	Avg. # multiplications per iteration	Avg. elapsed time per iteration (sec): [assignment, update] <sup>†</sup>	Maximum memory size (GB)
ES-ICP	$2.411 \times 10^{10}$	15.83 [5.466, 10.50]	7.914
ICP	$3.947 \times 10^{11}$	68.13 [57.22, 11.05]	4.147
CS-ICP	$2.137 \times 10^{10}$	86.16 [76.89, 9.380]	8.419
TA-ICP	$2.909 \times 10^{11}$	107.6 [94.44, 13.32]	8.645

<sup>†</sup> The average elapsed time does not exactly match the sum of the assignment and the update time because the algorithm terminated at the end of the assignment step of the last iteration.

TABLE XVIII  
PERF RESULTS OF ES-ICP, ICP, CS-ICP, AND TA-ICP IN 1M-SIZED NYT DATA SET WITH K=10000.  
NUMBER OF ITERATIONS UNTIL CONVERGENCE IS 81.

Algorithm	# instructions	# branches	# branch misses (%)	# LLC-loads	# LLC-loads misses (%)
ES-ICP	$7.041 \times 10^{13}$	$1.246 \times 10^{13}$	$4.094 \times 10^{10}$ (0.33)	$8.340 \times 10^{11}$	$1.051 \times 10^{11}$ (12.6)
ICP	$4.065 \times 10^{14}$	$4.363 \times 10^{13}$	$5.652 \times 10^{10}$ (0.13)	$4.734 \times 10^{12}$	$4.196 \times 10^{11}$ (8.86)
CS-ICP	$3.437 \times 10^{14}$	$4.322 \times 10^{13}$	$6.778 \times 10^{10}$ (0.16)	$5.783 \times 10^{12}$	$1.456 \times 10^{12}$ (25.18)
TA-ICP	$4.264 \times 10^{14}$	$5.876 \times 10^{13}$	$4.321 \times 10^{11}$ (0.74)	$6.894 \times 10^{12}$	$2.103 \times 10^{12}$ (30.50)

TABLE XIX  
PERFORMANCE COMPARISON OF MIVI, ES-, CS-, AND TA-MIVI IN 8.2M-SIZED  
PUBMED DATA SET WITH K=80 000.  
NUMBER OF ITERATIONS UNTIL CONVERGENCE IS 64.

Algorithm	Avg. # multiplications per iteration	Avg. elapsed time per iteration (sec): [assignment, update] <sup>†</sup>	Maximum memory size (GB)
MIVI	$1.326 \times 10^{13}$	3302 [3278, 23.81]	8.251
ES-MIVI	$3.562 \times 10^{11}$	266.7 [237.8, 29.38]	16.69
CS-MIVI	$7.601 \times 10^{11}$	2760 [2733, 27.53]	18.28
TA-MIVI	$3.856 \times 10^{12}$	3380 [3342, 37.99]	17.21

<sup>†</sup> The average elapsed time does not exactly match the sum of the assignment and the update time because the algorithm terminated at the end of the assignment step of the last iteration.

TABLE XX  
PERF RESULTS OF MIVI, ES-, CS-, AND TA-MIVI IN 8.2M-SIZED PUBMED DATA SET WITH K=80 000.  
NUMBER OF ITERATIONS UNTIL CONVERGENCE IS 64.

Algorithm	# instructions	# branches	# branch misses (%)	# LLC-loads	# LLC-loads misses (%)
MIVI	$1.024 \times 10^{16}$	$1.014 \times 10^{15}$	$3.929 \times 10^{11}$ (0.04)	$2.790 \times 10^{14}$	$1.767 \times 10^{13}$ (6.33)
ES-MIVI	$1.062 \times 10^{15}$	$1.677 \times 10^{14}$	$1.842 \times 10^{11}$ (0.11)	$3.592 \times 10^{13}$	$4.522 \times 10^{12}$ (12.6)
CS-MIVI	$9.065 \times 10^{15}$	$1.042 \times 10^{15}$	$6.201 \times 10^{11}$ (0.06)	$3.073 \times 10^{14}$	$2.711 \times 10^{13}$ (8.82)
TA-MIVI	$4.824 \times 10^{15}$	$6.895 \times 10^{14}$	$7.428 \times 10^{12}$ (1.08)	$1.754 \times 10^{14}$	$6.626 \times 10^{13}$ (37.77)

TABLE XXI  
PERFORMANCE COMPARISON OF MIVI, ES-, CS-, AND TA-MIVI IN 1M-SIZED NYT  
DATA SET WITH K=10 000.  
NUMBER OF ITERATIONS UNTIL CONVERGENCE IS 81.

Algorithm	Avg. # multiplications per iteration	Avg. elapsed time per iteration (sec): [assignment, update] <sup>†</sup>	Maximum memory size (GB)
MIVI	$1.955 \times 10^{12}$	272.4 [263.8, 8.723]	4.134
ES-MIVI	$9.411 \times 10^{10}$	26.06 [15.64, 10.55]	7.907
CS-MIVI	$7.536 \times 10^{10}$	346.7 [337.2, 9.568]	8.412
TA-MIVI	$1.367 \times 10^{12}$	280.6 [267.2, 13.56]	8.030

<sup>†</sup> The average elapsed time does not exactly match the sum of the assignment and the update time because the algorithm terminated at the end of the assignment step of the last iteration.

TABLE XXII  
PERF RESULTS OF MIVI, ES-, CS-, AND TA-MIVI IN 1M-SIZED NYT DATA SET WITH K=10 000.  
NUMBER OF ITERATIONS UNTIL CONVERGENCE IS 81.

Algorithm	# instructions	# branches	# branch misses (%)	# LLC-loads	# LLC-loads misses (%)
MIVI	$1.804 \times 10^{15}$	$1.716 \times 10^{14}$	$7.717 \times 10^{10}$ (0.04)	$2.720 \times 10^{13}$	$2.077 \times 10^{12}$ (7.64)
ES-MIVI	$1.518 \times 10^{14}$	$2.003 \times 10^{13}$	$7.343 \times 10^{10}$ (0.37)	$3.090 \times 10^{12}$	$2.774 \times 10^{11}$ (8.98)
CS-MIVI	$1.540 \times 10^{15}$	$1.766 \times 10^{14}$	$1.287 \times 10^{11}$ (0.07)	$2.907 \times 10^{13}$	$6.011 \times 10^{12}$ (20.68)
TA-MIVI	$1.851 \times 10^{15}$	$2.393 \times 10^{14}$	$1.677 \times 10^{12}$ (0.70)	$2.101 \times 10^{13}$	$3.689 \times 10^{12}$ (17.56)